TÉCNICO LISBOA

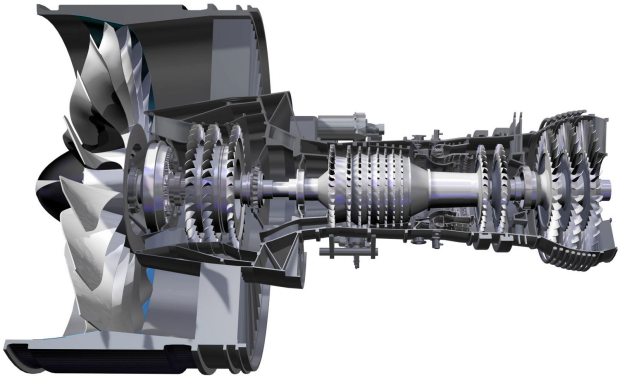

Turbofan Engine Optimization for Low NO_x Emissions

Francisco Mirpuri Matias

Thesis to obtain the Master of Science Degree in

Mechanical Engineering

Supervisors: Prof. João Manuel Melo de Sousa
Prof. Mário Manuel Gonçalves da Costa

Examination Committee

Chairperson: Prof. João Rogério Caldas Pinto
Supervisor: Prof. Mário Manuel Gonçalves da Costa
Member of the Committee: Prof. Cláudia Sofia Séneca da Luz Casaca

September 2016

Acknowledgments

I would like to use this section to thank everyone who contributed with moral and physical support throughout the making of this thesis. A special thanks goes to my family who implemented the seed of aviation from the beginning of my educational life leading to the stage i am today. A very special thanks goes to my partner in crime, Catarina, who always stood by my side cheering me up even in the least inspiring moments, lifting me to a more confidant self. And lastly to my dog, Spike, which literally stood by my feet throughout every line written in this thesis.

Abstract

More stringent limits for pollutants emissions are imposed to accommodate the experienced growth in the world's aircraft fleet. The most regulated of these pollutants are the nitrogen oxides, NO_x. These represent a health and environmental hazard, when emitted at both low and high altitudes. To reduce emissions without reducing engines performance presents a difficult task for engine design engineering. In order to do so, early-stage design tools are used to compute fast and realistically accurate results. These tools include the formulation of the models under the 0D framework. Following this approach, a 0D model of a two-spool turbofan was formulated and validated by comparing the results with those obtained from commercially available software. A combustion model was also formulated under the 0D framework, and validated by comparing its results with those presented in the literature. Two turbo-emissions models were achieved, one by unifying both turbofan and combustion models, and the second by coupling the turbofan model with a semi-empirical NO_x predictions model. Both models were validated by comparing the results with available data from the literature. The second unified model was used under an optimization algorithm in order to compute optimized parameters with the objective of low NO_x emissions while maintaining a low specific fuel consumption. To better understand the effects of the optimization in the combustion mechanism, the optimized parameters were computed through the more detailed turbo-combustion model.

Keywords

Turbofan Engine Model 0D, Combustion Model 0D, NO_x Emissions, Parametric Design Optimization

Resumo

Limites cada vez mais restritos para as emissões de poluentes são impostos de forma a acomodar o crescimento que a frota aérea mundial tem apresentado. Os mais regulados destes poluentes são os óxidos de azoto, NO_x. Estes representam um risco para a saúde e para o ambiente, quando emitidos tanto em baixas como altas altitudes. Reduzir as emissões de poluentes sem sacrificar o desempenho, apresenta ser um desafio para a concepção do motor. Para o fazer, são utilizadas ferramentas de projecto de forma a obter resultados realistas numa fase preliminar. Estas ferramentas incluem a formulação de modelos sob o formato 0D. Seguindo esta abordagem, um modelo de um turbofan de eixo duplo foi formulado, e validado comparando os resultados com os obtidos utilizando um software disponível comercialmente. Um modelo de combustão foi também formulado, e validado através da comparação dos resultados com aqueles presentes na literatura. Foram formulados dois modelos de turbo-emissões, o primeiro composto pelos modelos de turbofan e de combustão propostos, e o segundo pelos modelos de turbofan e semi-empírico de previsão de NO_x. Ambos os modelos são validados através da comparação dos resultados com os dados disponíveis na literatura. O segundo modelo de turbo-emissões foi acoplado a um algoritmo de optimização de forma a computar parâmetros de projecto optimizados com o objectivo de obter baixas emissões de NO_x enquanto mantendo um consumo especifico baixo. Para melhor entender os efeitos desta optimização no mecanismo de combustão, os parâmetros optimizados foram computados através do modelo mais detalhado de turbo-combustão.

Palavras Chave

Modelo de Turbofan 0D, Modelo de Combustão 0D, Emissões de NO_x, Optimização Paramétrica em Condições de Projecto

Contents

List of Figures

List of Tables

Abbreviations

CAEP Committee on Aviation Environmental Protection

CFD Computational Fluid Dynamics

CH_4 Methane

CO_2 Carbon Dioxide

CPR Compressor Pressure Ratio

DLN Dry Low NO_x

EI Emission Index

FESG Forecasting and Economic Analysis Support Group

FPR Fan Pressure Ratio

GE General Electric

GHG Green House Gases

GWP Global Warming Potential

H_2O Water Vapor

UHC Unburned Hydrocarbons

HPS High Pressure Shaft

HPT High Pressure Turbine

ICAO International Civil Aviation Organization

ISA International Standard Atmosphere

LPP Lean Pre-mixed Pre-vaporized

LPS Low Pressure Shaft

LPT Low Pressure Turbine

N_2O Nitrous Oxide

NO_2 Nitrogen Dioxide

NO_x Nitrogen Oxides

NO Nitrogen Monoxide

O_3 Ozone

OPR Overall Pressure Ratio

PM Particulate Matter

RQL Rich burn, quick Quench, Lean burn

SO_2 Sulfur Dioxide

SO_4 Sulfate

SO_x Sulfur Oxides

TAPS Twin-Annular Premixed Swirler

TIT Turbine Inlet Temperature

TVC Trapped Vortex Combustor

List of Symbols

A	Area, m^2
B	Bypass ratio
c	Speed of sound, m/s
c_p	Air specific heat at constant pressure, J/kgK
c_{pg}	Combustion gases specific heat at constant pressure, J/kgK
E	Total energy, J
f	Fuel-to-air ratio
g	Acceleration of gravity, m/s^2
h	Specific enthalpy, kJ/kg
H	Altitude, m
HV	Lower heating value, J/kg
k	Rate constant
K_p	Equilibrium constant
$\dot{m}_a$	Air mass flow, kg/s
$\dot{m}_f$	Fuel mass flow, kg/s
M_0	Mach number
P	Static pressure, atm
P_t	Total pressure, atm
Q	Heat exchanged, J
R	Air specific gas constant, J/kgK
s	Specific entropy, J/Kkg
t_i	Residence time, ms
T	Static temperature, K
T_t	Total temperature, K
T_N	Nominal Thrust, kN
u_0	Flight velocity, m/s
u	Specific internal energy, kJ/kg
ν	Stoichiometric coefficient
W	Work, J
y	Mole fraction
η	Isentropic efficiency
η_p	Politropic efficiency
γ	Air heat capacity ratio
γ_g	Combustion gases heat capacity ratio
ρ	Density, kg/m^3
Φ	Equivalence ratio
Ψ	Specific thrust, s

Subscripts

b	Combustor
c	Compressor
d	Diffuser
f	Fan
m	Mechanical
n	Nozzle
pz	Primary zone
$r*$	Ram recovery
st	Stoichiometric

1

Introduction

Contents

In this chapter, the motives that led to the presentation of this work are presented, as well as the state of the art in current technology and research, and lastly, the objectives and outline of the present thesis.

1.1 Motivation

With an increasing interest in global interactions and communications, airline traveling and freight transport becomes a primary necessity for those who want to be in line with progress. Data collected by the Forecasting and Economic Analysis Support Group (FESG) of the International Civil Aviation Organization (ICAO) Committee on Aviation Environmental Protection (CAEP), foreseen a great increment in air traffic and environmental footprint in a 30-year time horizon. In Most Likely scenarios, which are used as a central forecast, data shows that the demand for this mean of transportation is expected to increase each year by an average of 4.9% for passenger traffic, and an average 5.2% for freight traffic for the next 15 years and in the 10 years after that, 4.0% and 4.6% respectively [1]. To accommodate the expected growth in air traffic, an increase of fleet size is inevitable. By 2040 it will be needed around 56'000 new airliners to commercial passenger traffic, 6'000 new aircraft to freight traffic and around 45'000 will be needed to business passenger traffic. Combining both passenger and freight operations, it is expected that the number of flights worldwide triple by 2040, as Table 1.1 summarize.

Table 1.1: CAEP/9 Forecast of Aircraft Operations (Millions).

Type of Operation	2010	2020	2030	2040
Passenger flights	28.5	43	60.9	82
Freight flights	1.6	2.3	3.2	4.4
Business aviation flights ($<$20 seats)	2.6	3.7	5.3	7.9
Total (World)	32.7	49	69.4	94.3

1.1.1 Environmental concerns

With such an increase in fleet and operations, an increase in environmental concerns are also to be expected and even more stringent throughout the years to come. Aircraft engines currently run on fossil-fuel which it combustion emit various pollutants to the atmosphere, affecting local and regional air quality, as well as affecting its cleanest regions at high altitude under cruise conditions, as presented in figure 1.1. Such emissions modify the chemical and microphysical properties of the atmosphere resulting in changes of Earth's climate system, which can ultimate in critical changes in our planet fragile ecosystem [6]. Of particular importance to the environment are the emissions of Carbon Dioxide (CO_2), Nitrogen Monoxide (NO) and Nitrogen Dioxide (NO_2) (collectively known as Nitrogen Oxides (NO_x)), Sulfur Dioxide (SO_2) and Sulfate (SO_4) (collectively know as Sulfur Oxides (SO_x)), Unburned Hydrocarbons (UHC), and Particulate Matter (PM). This emissions pose great source of concern as the major product of the combustion, CO_2, is the most significant Green House Gases (GHG) emitted that influence climate change and in addition emission of: NO_x result in the production of Ozone (O_3) and Methane (CH_4), which are associated with changes in the oxidizing

capacity of the atmosphere [7] [8]; Water Vapor (H_2O) and PM play a role in the formation of contrails and potential modification of cirrus clouds [9]; and SO_x and UHC which are responsible for aerosol production and heterogeneous chemistry [10]. It is also important to consider the potential effect of supersonic aircraft fleet operation in stratospheric ozone layer [7].

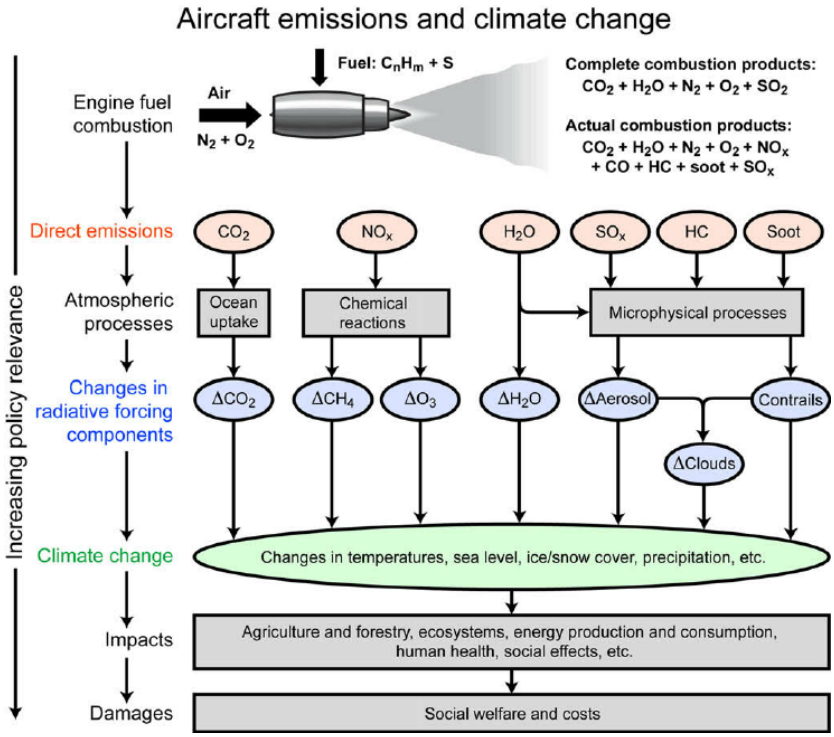

Figure 1.1: Schematic of the Principal Emissions from Aviation Operations and the Relationship of Emissions to Climate Change and Impacts. The terminology, ΔX, indicates a change in component X. The term, Δclouds, represents contrail cirrus and potential changes from other cloud effects. [1]

NO_x Emissions

In special focus for this work is NO_x emissions from subsonic aircraft engines. When locally emitted, exposes great concern as it can lead to the formation of other pollutants, such as particulates and ground-level ozone, which are harmful to health, thus contributing to a wide range of respiratory and heart diseases [11]. NO_x also prove to be danger the environment by causing the eutrophication [12] and acidification of water and soils. When emitted at cruise altitudes, at the upper tropospheric layer, the production of NO_x leads to, the formation of ozone, by a photochemical processes, and the reduction in CH_4 concentration, which are both GHG. These two processes have opposite effects concerning radioactive forcing, and when combined, the estimated radioactive forcing of NO_x can be considered 100 to 130 times more powerful than CO_2 when concerning global warming effects (100-130 Global Warming Potential (GWP)). Although indirectly, NO_x can also be responsible of emitting Nitrous Oxide (N_2O), which as a 298 GWP [13].

1.1.2 Restrictions

To reduce polutant emissions by the aerospace industry the CAEP, which is responsible for formulating new standards in aircraft noise and emissions regulations, established limits addressing local

air quality in the vicinity of the airports based on a LTO cycle analysis. Although regulations have been established to reduce emissions of UHC, CO, smoke and PM the primary focus of the international council as been a more stringent NO_x emission limits. In 1981 the first standard for NO_x emissions was adopted and CAEP have been periodically introduced more stringent NO_x limits, as seen in Figure1.2, which are commonly referenced by the number of the CAEP meeting in which they have been established (i.e. CAEP/2, CAEP/4, CAEP/6 and CAEP/8), while CAEP limits for UHC and soot have not been changed from their original value as they are considered to provide adequate environmental protection.

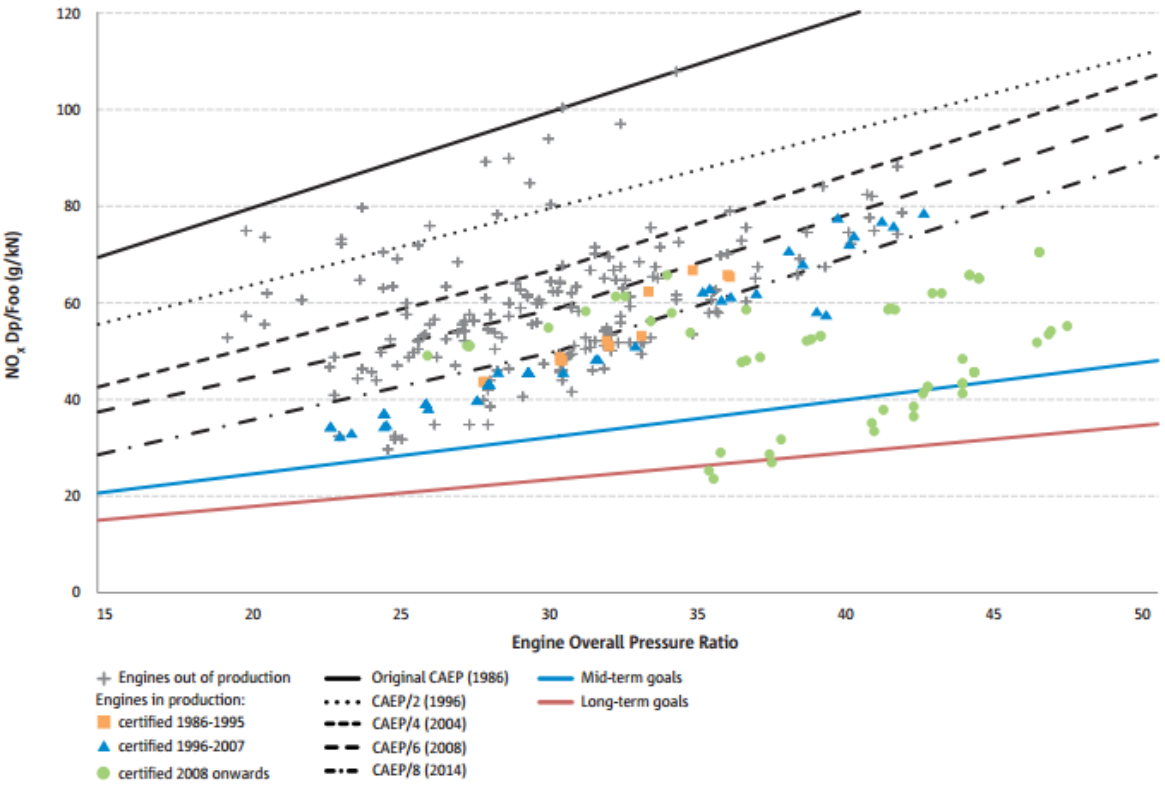

Figure 1.2: Continuous improvement in NO_x emissions regulations over time.[2]

It is also important to refer the trade-offs undergoing in the industry in order to reduce NO_x emissions. To better decrease CO_2 emissions, the industry tends to increase engine temperatures and pressure which increase thermal and fuel efficiency, by doing this less fuel will be consumed and CO_2 emissions will be reduced, on the other side an increase in temperature will lead to an increase in NO_x emissions. For this matter, it is important to weight in the NO_x:CO_2 trade-offs, as well as noise reduction in future technological advancements [14]. Despite the difficulties that trade-offs add to engine design, technology have been advancing in order to reduce the amount of fuel burn and NO_x production 1.3.

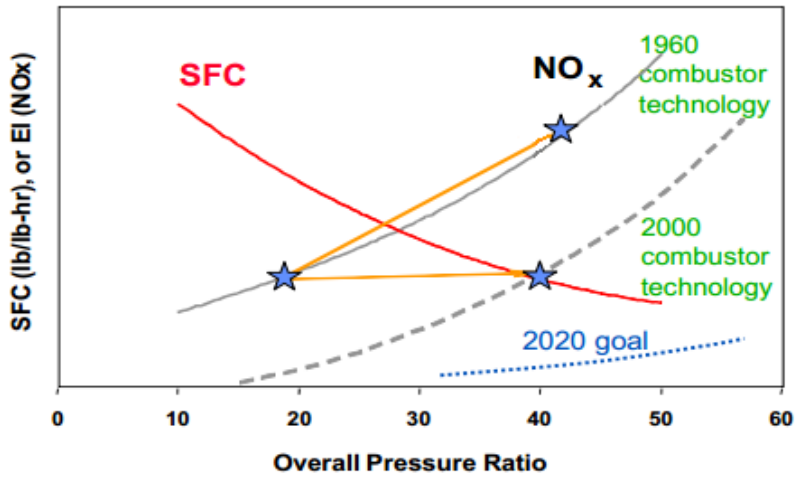

Figure 1.3: Illustration of the evolution of combustion technology regarding NO_x:SFC tread-offs (adapted from [3])

1.1.3 Predictions

In order to design an overall efficient aircraft it is needed a considerate amount of effort to be put in the design of the gas turbine engine. Important design requests have to be taken into account, such as thrust, fuel consumption, pollutants emissions, dimensions, noise level, etc.. Combustor design is responsible for a big portion of the design effort as it is where the combustion takes place and, for that reason, the most physically complex phenomena are presented. To greatly reduce the cost of research in this field, a computational approach is needed in order to alleviate the effort in experimental procedures. Although a computational approach is preferable, it still poses a great deal of work and effort to achieve sufficiently precise model of the combustion phenomena. Models studying the complex 3 Dimensional (3D) flow field and chemical reactions altogether are very computational demanding and time consuming. It is also still too difficult, with the current computational methods, a complete theoretical treatment of the simultaneous involvement of fuel spray atomization and vaporzation, finite rate chemistry of combustion, pollutant formation, radiation, particle behavior, turbulent transport and recirculation zones involving multiple flow streams. For this matter, it is of use less computationally demanding methods to predict the desired output. Simpler and faster methods like 0D computational models and empirical formula provide a good alternative in an early stage design, as they tend to deliver a good approximation for a fraction of the effort, as they describe the flow throughout the various components with simple isentropic evolution equations. It is also important to refer that such empirical formula derived from correlation with experimental data sets, while analytical models (0D-3D models) are discretized versions of the governing equations. This imply that empirical formula, although produces faster and more accurate results, are only applicable in similar conditions to those of the data used to formulate then, and consequently are less flexible regarding new designs. On the other side, analytical and heavily computational 3D models, although less accurate, are more flexible and ultimately the only tool for producing new designs. In order to compromise, semi-empirical and 0D models can be achieved with both fast and accurate results.

1.2 State of The Art

In this chapter it will be mention the state of current work in the gas turbine design, with special focus on combustor design and prediction models for NO_x emissions.

1.2.1 Current Technologies and Research

As stated before, the main focus of manufactures lays in the design of an engine combustor capable of reduced emissions while maintaining or increasing thermal and fuel efficiency. This effort led to the development of a wide range of technologies involving different approach on how pollutant can be reduced. One way of reducing emissions is to inject water or steam into the combustor, although this method is not appropriate in aircraft engines as it adds complexity and weight that aircraft designers can't afford. For this matter Dry Low NO_x (DLN) combustors had to be design in order to reduce emissions without 'wet' water injections. Combustor designers used to rely on diffusion flame combustor technology, as this type of flame tends to provide a more stable flame at various loads, which is an important aspect in aircraft engine applications, and higher flame temperatures, which provide a higher thermal efficiency and therefore reduced fuel consumption. But also, as mention before, high flame temperatures lead to a higher NO_x emissions, which is a downfall. With the development of premixed combustion systems, combustion can take place at a much lower equivalency ratio where flame temperature is lower and therefore NO_x emissions can be minimized.

Technology in a diffusion flame combustor, namely Rich burn, quick Quench, Lean burn (RQL), avoid to operate in stoichiometric conditions, burning initially a rich mixture, then quick quenching the flame and followed by burning the remaining fuel at lean conditions as illustrated at 1.4.

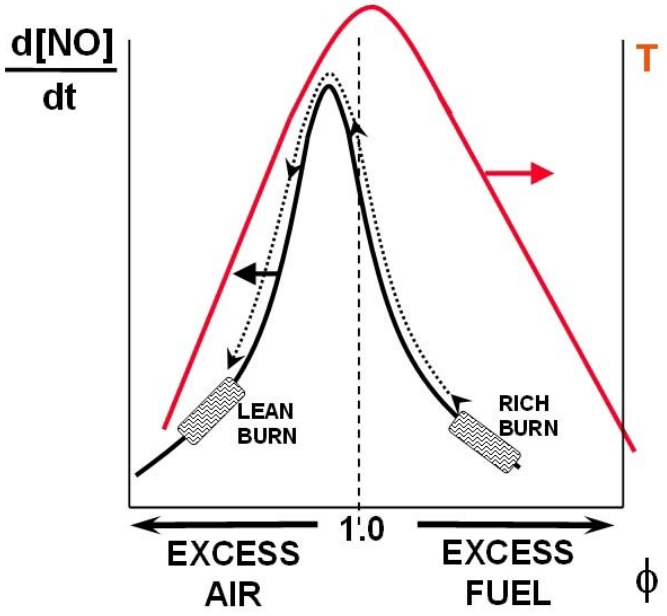

Figure 1.4: Example Rich-Quench-Lean Combustion process.[4]

Current RQL combustors have high levels of efficiency at all high-power operating points [15],

this successful performance relies on quick turbulent mixing providing a uniform mixture and good fuel atomization [16]. The importance of turbulent mixing in RQL design led to research upon its improvement. Experimental research was conducted by Jermakian et al. [17], reporting the effects of elevated pressure and temperature on jet mixing and emissions in an RQL combustor. Computational Fluid Dynamics (CFD) research was also conducted in order to investigate the performance of RQL combustors [18–21], as well as less computationally demanding 1D model conducted by Marvis et al. [22], with a more detailed flow model throughout the combustor when comparing with the 0D model approach.

Research made by General Electric (GE) led to the development of Twin-Annular Premixed Swirler (TAPS) combustor, which take advantage of premixed and lean-burn flames (i.e. Lean Pre-mixed Pre-vaporized (LPP) combustors). As mention, for this type of combustor, the primary zone of reaction is kept lean, resulting in low combustion temperatures and NO_x emissions, thus sacrificing flame stability. To counter this effect, two co-annular swirling jets are produced by the pilot and main mixer [23]. Fuel staging is used in the fuel nozzle to control fuel distribution from the center pilot, which have a rich configuration similar to traditional combustors, and the main mixer, which is composed by a set of radial jets that enter the main air swirler. This configuration allows that at idle and low power operations the fuel circulates mainly through the pilot providing flame stability and at higher power climbing and take-off operations, a mixture of the main (90%-95%) and pilot (5%-10%) jets is used in order to burn the fuel in lean conditions. The benefits of this type of technology can be seen as illustrated in 1.5. Numerical research as been performed by Matuszewki et al. [24] regarding NO formation in multi-point combustion chamber and a 1D model was also assessed by Marvis et al. [22].

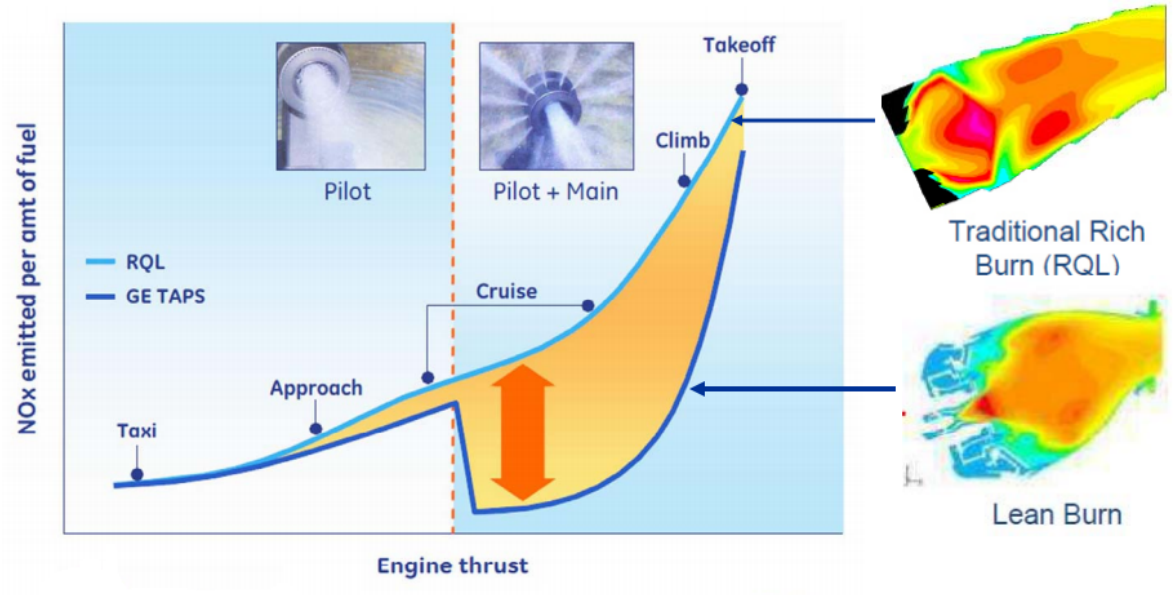

Figure 1.5: Illustration of NO_x flight cycle comparison between RQL and TAPS combustor technologies by GE [5]

Other promising technologies like Trapped Vortex Combustor (TVC) rely on trapped vortex created by a cavity stabilization concept. Recirculation zones are created allowing the mixture of hot products

of combustion and reactant at high rate, and promoting flame stability [25]. An efficiently mixed mixture of reactants are provided by the turbulence occurring in the ”trapped” vortex, where part of reaction takes place, resulting in a ”typically” flameless regime and contributing to a significant reduction in pressure drop [26]. TVC has the advantage of being capable of operating as a staged combustor and potentially achieving about 10% to 40% reduction in NO_x emissions [27], and also the advantage of being capable operating as a RQL combustor, benefiting from the advantages of this kind of combustion system [28]. Research with this type of combustor have been performed by Xing et al. [29, 30] in lean blow-out and performance, and a new design for lean-premixed TVC was proposed by an experimental research led by Bucher et al. [31].

1.2.2 Semi-empirical Models

Semi-empirical models are usually a great tool for an accurate prediction of pollutant emissions. These models also prove to be more useful than their computationally expensive counterparts as, at the early stage of design, the amount of input data (i.e. boundary conditions) is reduced, making it the preferred choice as a conceptual design tool. Several semi-empirical models have been produced over the years in order to accommodate combustor design features, combustor dimensions, operating conditions, fuel type and fuel spray characteristics, as well as technology advancements. The exhaust concentration of pollutants are assumed, by Lefebvre [32], to be dependent of three parameters: mean residence time in the combustion zone, chemical reaction rates and mixing rates. The following expressions were than derived from those parameters in terns of combustor size, pressure drop, airflow proportions and combustor inlet conditions [33].

Lefebvre

Research conducted by Lefebvre [32] propose equation (1.1) based on experimental data from various aero-engine combustors.

$$NO_x = 9 \times 10^{-8} P^{1.25} V_c exp(0.01 T_{st}) / \dot{m} T_{pz} \quad \text{g/kg fuel} \tag{1.1}$$

This equation takes account that in diffusion flames, the formation of NO_x is determined not by the average flame temperature, T_{pz}, but by the stoichiometric flame temperature, T_{st}. On the other hand, residence time is represented in this equation by the average flame temperature. Equation (1.1) is only suitable for conventional spray combustors and can be used for LPP combustors by substituting T_{st} by T_{pz}, which is the maximum attainable temperature in this type of combustors.

Rizk $\&$ Mongia

Rizk $\&$ Mongia [34] formulated a model in which the combustor is defined by a number of reactors that simulate different zones within the combustor, namely: near the wall zones, Lean Blow Out zone, primary zone, secondary/intermediate zone and dilution zone. A set of equations were then proposed for NO_x emissions in the primary zone, where the highest temperature of combustion is achieved.

$$NO_x = 10^{13} \left(\frac{p_{t3}}{1.4 \times 10^6}\right)^{aa} exp(-71442/T_{pz})(7.56\Phi^{-7.2} - 1.6) t^{0.64} \quad \text{g/kg fuel} \tag{1.2}$$

For $\phi > 1.08$ the following equation was formulated:

$$NO_x = 10^{13}\left(\frac{p_{t3}}{1.4\times10^6}\right)^{aa} exp(-71442/T_{pz})(5.21\Phi^{-2.99} - 1.6)t^{0.64} \quad \text{g/kg fuel} \tag{1.3}$$

In downstream zones of the combustor where the temperature is still high enough to the formation of additional NO_x, an expression was also formulated:

$$NO_x = 10^{14}\left(\frac{p_{t3}}{1.4\times10^6}\right)^{aa} exp(-71442/T_{pz})(1.172\Phi^{-4.56} - 0.6)t^{0.876} \quad \text{g/kg fuel} \tag{1.4}$$

where the term aa is given by:

$$aa = 11.949exp\left(-\frac{\Phi}{5.76}\right) - 10.0 \tag{1.5}$$

Rizk and Mongia also formulated equation (1.6), in which fuel vaporization is taken into account by the introducing the term t_e.

$$NO_x = 15\times10^{14}(t - 0.5t_e)exp(-71100/T_{st})P^{-0.05}(\Delta P/P)^{-0.5} \quad \text{g/kg fuel} \tag{1.6}$$

The equation state that a reduction of mean drop size will result in an increase in NO_x emissions by reducing the fuel vaporization time, but it was also observed that, if vaporization time is negligible in comparison with the total residence time, the reduction of mean drop size would result in a reduction in NO_x emissions [35].

Kyprianidis et al.

Recent research also led by Kyprianidis et al. [36] produced the derivation of a semi-empirical correlation of NO_x emissions for modern RQL combustors.

$$NO_x = (a + b\times e^{(cT_{31})})\left(\frac{P_{31}}{P_{31,ref}}\right)^d e^{f(h_{SL}-h)}\left(\frac{\Delta T_{comb}}{\Delta T_{comb,ref}}\right)^{TF} \tag{1.7}$$

Equation (1.7) was derived for a modern RQL single-annular design to operate at high overall pressure ratios engines. This equation has predictive capability as it was based on large number of engine performance models using in-house library and has also been verified for high overall pressure ratio turbofan designs with technology levels consistent with the year of entry into service around 2020 [37].

Various other models for semi-empirical correlations for NO_x emissions here produced and can be found in literature, namely Mellor [38] for correlations developed before 1980, Lewis [39] for lean and homogeneous combustion, Odgers and Kretschmer [40], Becker and Perkavec [41], Nicol et al. [42], Madden and Park [43] for the P3T3 Model which provides correction of ground level measurements for conditions at altitude and research done by the Committee of Aeronautical Technologies [44] which proposed a severity parameter in order to define NO_x emissions.

1.3 Objectives

The objective of the present work lies on the optimization of the design parameters of a turbofan in order to reduce NO_x formation at the high temperatures achieved in the primary zone of the combustor. In order to compute such optimization it is necessary to develop parametric models of the turbofan and combustion phenomena.

The thermodynamic model of a turbofan should be developed under a 0D framework and provide realistic results. The validation of the model should be taken care by the comparison of the obtained results with those obtained from a recognized commercial software, such as GasTurb®, and by comparing the obtain performance parameters with those retrieved from ICAO data bank. A chemical reaction model of the primary zone needs to be formulated in order to assess the NO_x formation mechanism. The primary zone combustion model will be submitted to validation by comparing the obtained emissions results with data from ICAO emissions data bank. Lastly, an optimization algorithm will be paired with the turbofan model in order to achieve optimized design parameters for low NO_x emissions.

1.4 Thesis Outline

The present thesis is divided in six chapters, including the present introduction chapter. In chapter 2, the thermodynamic model of a two-spool turbofan is assessed. It is presented a brief introduction, as well as the equations of the thermodynamic processes which the working fluid undergoes at each component of a turbofan. Results from this model are presented and validated for various input parameters. In chapter 3, a theoretical approach to a hydrocarbon combustion is studied as well as the NO_x formation mechanism, leading to the development of the primary zone combustion model with focus in NO_x prediction. The results of the combustion model are presented and validated for different conditions. In chapter 4, the thermodynamic model of a turbofan is paired with the proposed primary zone combustion model as well as a NO_x prediction model from the literature. Results of these conjoint models are computed and compared with data from the literature. In chapter 5, the optimization process is formulated and the results presented. In chapter 6, the conclusions of the present work are presented.

2

Thermodynamic Model

Contents

The present chapter refers to the modeling of the turbofan thermodynamic cycle, with special focus on the modeling of the atmospheric air and the components within the aircraft engine in study.

2.1 Environment Modeling

The environment where the aircraft is inserted is of major relevance to the overall design of its structure and engines. Particularly in the case of the engine, the air is the working fluid running trough all its core components, reaching rates of consumption in the order of thousands of kilograms of air per second. Therefore, an accurate model of the fluid conditions is in order to achieve a realistic parametric analysis.

2.1.1 Atmospheric Air

The atmospheric air is modeled through the International Standard Atmosphere (ISA) model [45], where the Earth's atmosphere temperature, pressure, density and viscosity vary with the aircraft operating altitude, H. Therefore the atmospheric air pressure and temperatures are computed as follows:

$$P_0 = f(H) \tag{2.1a}$$

$$T_0 = f(H) \tag{2.1b}$$

2.1.2 Flight Mach Number and Aircraft Velocity

By using the above computed air proprieties, the speed of sound can by defined by,

$$c = \sqrt{\frac{\gamma R T_0}{M_{air}}} \tag{2.2}$$

where γ is the isentropic expansion factor given by the ratio between specific heat of the air at constant pressure, c_p, and the specific heat at constant volume, c_v. With the speed of sound calculated, the aircraft velocity can be expresses by,

$$u_0 = M_0 \times c \tag{2.3}$$

The aircraft velocity is used as the velocity of the approaching air when considering the plane at a fixed referential. The air velocity is then used in order to compute the specific thrust.

2.2 Turbofan Modeling

In this section is performed a model overview throughout each component of a tow-spool Turbofan engine with separated exhaust flows. The model includes:

- Inlet
- Fan
- Compressor

- Combustor
- Turbine
    1. High Pressure Turbine
    2. Low Pressure Turbine
- Nozzles
    1. Bypass Nozzle
    2. Core or Exhaust Nozzle
- Thrust and Thrust Specific Fuel Consumption

The following figure will be used throughout the thesis as a reference of the stage numbering within the Turbofan.

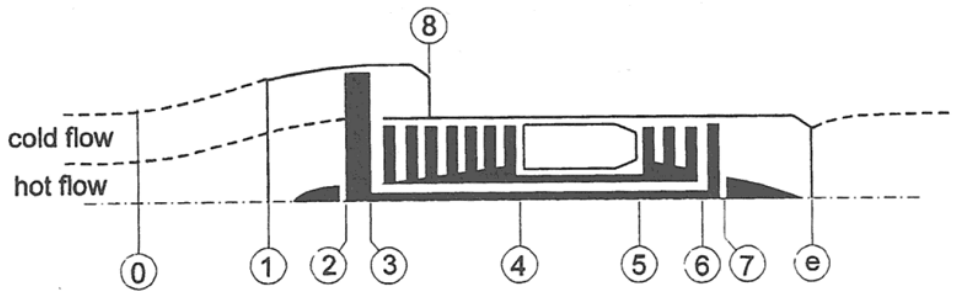

Figure 2.1: Turbofan stage numbering.

2.2.1 Inlet

At operating conditions the inlet have to ensure a reduction of the air velocity coming into the engine so it can take a level suitable for the compression process taking place in the fan, from $M_0 = 0.4$ to 0.7 otherwise a use of a transonic fan is needed. This reduction has to be achieved with the lowest possible losses in stagnation pressure. It also have to delay as much as possible the separation of the boundary layer of the inside flow as well as the outside flow. The separation might be caused by a deviation of the incoming flow and the inlet, so the performance of the inlet should be as independent as possible of the attack angle. The inlet should ensure a uniform flow at the fan's entry surface avoiding to penalize the performance. The inlet design has to account for a spectrum of traveling velocities, making it difficult if $M_0 \geq 1$, as it must take into account the highly inefficient effects of the shock waves that take place inside and outside the fuselage of the inlet.

Inlet Model

The inlet can be assumed to be adiabatic, so the stagnation temperature of the incoming air T_{t0} is equal to stagnation temperature at the fan's entry surface T_{t2}. The T_{t0} can be taken from an isentropic process, thus:

$$T_{t0} = T_0 + \frac{u_0^2}{2cp} = T_0(1 + \frac{\gamma - 1}{2}M_0^2) = T_{t2} \tag{2.4}$$

Stagnation pressure drops occur in the inlet because of boundary layer effects and from shock waves. Both effects can be taken into account using one of the two following definitions:

- Isentropic efficiency, η_d

$$\eta_d = \frac{h_{t2s} - h_0}{h_{t0} - h_0} \cong \frac{T_{t2s} - T_0}{T_{t0} - T_0} \tag{2.5}$$

The values for η_d can be taken from tables with typical values for different type of inlet designs and can then be related with the pressure drop by:

$$\frac{P_{t2}}{P_0} = \left[1 + \eta_d\left(\frac{\gamma - 1}{2}\right)M^2\right]^{\frac{\gamma-1}{\gamma}} \tag{2.6}$$

- Pressure recovery factor, π_d

$$\pi_d = \pi_{dmax}\eta_r \tag{2.7}$$

where π_{rmax} represents the percentage of π_d that comes from the effects of the boundary layer and η_r represents the percentage of π_d due to shock wave losses. Like η_d, values for π_{rmax} can also be take from tables. For η_r a useful reference is Military Specification 5008D [46].

$$\eta_r = \begin{cases} 1 & M_0 \leq 1 \\ 1 - 0.075(M_0 - 1)^{1.35} & 1 < M_0 < 5 \\ \frac{800}{M_0^4 + 935} & 5 < M_0 \end{cases}$$

Although, at operating velocities of the engine in study, almost always $M_0 \leq 1$ so the contribution of η_r will be negligible. The parameter can then be related with the pressure drop by:

$$\frac{P_{t2}}{P_0} = \pi_d\left[1 + \left(\frac{\gamma - 1}{2}\right)M^2\right]^{\frac{\gamma-1}{\gamma}} \tag{2.8}$$

The relationship between both parameters that are presented can be given by:

$$\eta_d = \frac{\left(1 + \frac{\gamma-1}{2}M^2\right)\pi_d^{\frac{\gamma-1}{\gamma}} - 1}{\frac{\gamma-1}{2}M^2} \tag{2.9}$$

2.2.2 Fan

The fan is responsible for propelling the air incoming from the inlet to the bypass duct, generating the majority of the engine's overall thrust, and to the compressor, making it a first stage of the air compression in the core flow.

Fan Model

At a design stage the Fan Pressure Ratio (FPR) is given, and can be written in terms of stagnation pressure ratio:

$$FPR = \frac{P_{t3}}{P_{t2}} \tag{2.10}$$

The temperature ratio can be taken from either a polytropic evolution, equation (2.12), or an isentropic evolution, equation (2.11).

$$\eta_f = \frac{h_{t3s} - h_{t2}}{h_{t3} - h_{t2}} \cong \frac{T_{t3s} - T_{t2}}{T_{t3} - T_{t2}} \tag{2.11}$$

$$n = \frac{\eta_{pf}\gamma}{\eta_{pf}\gamma - \gamma + 1} \tag{2.12}$$

where n the exponent of the polytropic process and η_{pf} the small stage efficiency or polytropic efficiency. Both efficiencies can then be related with the stagnation temperature ratio as following:

$$\frac{T_{t3}}{T_{t2}} = 1 + \frac{1}{\eta_f}\left[\left(\frac{P_{t3}}{P_{t2}}\right)^{\frac{\gamma-1}{\gamma}} - 1\right] \tag{2.13}$$

for isentropic efficiency and

$$\frac{T_{t3}}{T_{t2}} = \left(\frac{P_{t3}}{P_{t2}}\right)^{\frac{\gamma-1}{\eta_{pf}\gamma}} \tag{2.14}$$

for polytropic efficiency. These efficiencies can also be related to each other by:

$$\eta_f = \frac{\left(\frac{P_{t3}}{P_{t2}}\right)^{\frac{\gamma-1}{\gamma}} - 1}{\left(\frac{P_{t3}}{P_{t2}}\right)^{\frac{\gamma-1}{\eta_{pf}\gamma}} - 1} \tag{2.15}$$

2.2.3 Compressor

The compressor is responsible for most of the compression of the core flow. In most applications in the interest of the thesis, the compression is taken care by axial compressors, which are composed by multiple stages, and each stage composed by a rotor and a stator. The compression is typically done by passing the working fluid at a constant axial velocity through a decreasing volume along the compressor stages, each stage in small compression ratios but high efficiency, increasing it's density. This will make for the combustion to take place in a smaller volume and better efficiency.

Compressor Model

As in the case of the fan, the Compressor Pressure Ratio (CPR) is given, and can be written in terms of stagnation pressure ratio:

$$CPR = \frac{P_{t4}}{P_{t3}} \tag{2.16}$$

It is also worthwhile define the Overall Pressure Ratio (OPR):

$$OPR = \frac{P_{t4}}{P_{t3}}\frac{P_{t3}}{P_{t2}} = \frac{P_{t4}}{P_{t2}} \tag{2.17}$$

The stagnation temperature ratio in the compressor can also be define as done in the fan, by an isentropic evolution:

$$\frac{T_{t3}}{T_{t2}} = 1 + \frac{1}{\eta_c}\left[\left(\frac{P_{t3}}{P_{t2}}\right)^{\frac{\gamma-1}{\gamma}} - 1\right] \tag{2.18}$$

or by an polytropic evolution:

$$\frac{T_{t4}}{T_{t3}} = \left(\frac{P_{t4}}{P_{t3}}\right)^{\frac{\gamma-1}{\eta_{pc}\gamma}} \tag{2.19}$$

2.2.4 Combustor

Of all the components of the engine, the combustor or burner might be the one with the most complex design and theoretical modeling, as it takes on problems such as complex fluid geometry, heat transfer and, most importantly, combustion. The combustor can have different designs: can-type, annular-type or can-annular-type. Although it can be said that all follow some basic concept, the combustor is formed by a diffuser and then three main stages, primary zone, intermediate zone and a dilution zone. The diffuser is responsible for decreasing the velocity of the compressed air, assuring that the flame does not blowout or blowoff. After the diffuser, just part of the air enters the primary zone, the other part goes around the the primary zone working as a cooling fluid for the hot surfaces and is then used in the intermediate and dilution zone. In the primary zone is where the main combustion reaction takes place, the fuel injectors provide the necessary amount of fuel so that the flame is within the flammability limits, usually achieving equivalence ratios from 0.8 to 1.2. In the intermediate zone, products of combustion and unburned fuel meet some of the cooling air, reducing the temperature of hot gases and providing the necessary oxygen to complete the combustion process and recover from dissociation losses. As in this stage unburned fuel is present at low amounts, the overall equivalence ratio vary from 0.4 to 0.6. In the final stage of the combustor, the rest of the cooling air is then mixed with the hot gases from the intermediate zone making sure that the gases at the inlet of the turbine are presented at the a specific designed temperature and the as homogeneous as possible. The pressure loss of the gases passing through the combustor should be as minimal as possible, although the high level of turbulence of the air mixing with the hot gases, wall friction and the increase of temperature by combustion itself, all cause pressure loss.

Combustor Model

The stagnation pressure losses through the burner, π_b, can be defined by:

$$\pi_b = \frac{P_{t05}}{P_{t04}} \tag{2.20}$$

Combustion efficiency, η_b, is defined by:

$$\eta_b = \frac{(\dot{m}_{ah} + \dot{m}_f)c_{pg}T_{t5} - \dot{m}_{ah}c_pT_{t4}}{\dot{m}_f HV} \tag{2.21}$$

It can also be defined the fuel to air ratio, f, on the core of the turbofan by:

$$f = \frac{\dot{m}_f}{\dot{m}_{ah}} = \frac{c_{pg}T_{t5} - c_pT_{t4}}{\eta_b HV - c_{pg}T_{t5}} \tag{2.22}$$

2.2.5 Turbine

The turbine is responsible for the exchange of mechanical energy with the hot gases coming from the combustor, providing the necessary energy to the compressor, the fan and the accessories. Most

of the turbines used in the aeronautical industry are axial turbines. In a two spool turbofan, as in the objective of this thesis, the turbine is divided in two segments: High Pressure Turbine (HPT) and Low Pressure Turbine (LPT), each with multiple stages. The HPT is the first to receive the hot gases from the combustor and it is responsible for the absorption of majority of the energy exchange with the gas, providing the necessary energy to the compressor trough the High Pressure Shaft (HPS). The first stage (formed by a stator and then a rotor, contrary to a compressor stage) of the HPT is responsible for limiting the combustor exit temperature, as it's in high rotational speeds, the centrifugal forces combined with the gases high temperatures, form a structural stress limit for the rotor blades. The rotor blades can be ventilated, cooling the blade material and increasing the allowed Turbine Inlet Temperature (TIT). The LPT then absorb some of the remaining of the kinetic energy of the gas providing energy to the fan and accessories trough the Low Pressure Shaft (LPS).

High Pressure Turbine Model

Given a design TIT, the stagnation temperature at the exit of the HPT can be computed trough the energy used at the compressor for the increase of enthalpy.

$$\eta_m \dot{m}_{ah}(1+f)c_{pg}(T_{t5}-T_{t6}) = \dot{m}_{ah}c_p((T_{t4}-T_{t3}) \tag{2.23}$$

$$T_{t6} = T_{t5} - \frac{c_p(T_{t4}-T_{t3})}{c_{pg}\eta_m(1+f)} \tag{2.24}$$

The stagnation pressure ratio can be defined by an isentropic evolution

$$\frac{P_{t6}}{P_{t5}} = \left[1 - \frac{1}{\eta_t}\left(1 - \frac{T_{t6}}{T_{t5}}\right)\right]^{\frac{\gamma_g}{\gamma_g - 1}} \tag{2.25}$$

or by a polytropic evolution

$$\frac{P_{t6}}{P_{t5}} = \left(\frac{T_{t6}}{T_{t5}}\right)^{\frac{\gamma_g}{(\gamma_g - 1)\eta_{pt}}} \tag{2.26}$$

Low Pressure Turbine Model

Like the in HPT, the stagnation temperature at the exit of the LPT can be computed be the energy used by the fan, mainly.

$$\eta_m \dot{m}_{ah}(1+f)c_{pg}(T_{t6}-T_{t7}) = \dot{m}_{at}c_p((T_{t3}-T_{t2}) \tag{2.27}$$

$$T_{t7} = T_{t6} - \frac{c_p(T_{t3}-T_{t2})(1+B)}{c_{pg}\eta_m(1+f)} \tag{2.28}$$

The stagnation pressure ratio can also be defined either by an isentropic evolution

$$\frac{P_{t7}}{P_{t6}} = \left[1 - \frac{1}{\eta_t}\left(1 - \frac{T_{t7}}{T_{t6}}\right)\right]^{\frac{\gamma_g}{\gamma_g - 1}} \tag{2.29}$$

or by a polytropic evolution

$$\frac{P_{t7}}{P_{t6}} = \left(\frac{T_{t7}}{T_{t6}}\right)^{\frac{\gamma_g}{(\gamma_g - 1)\eta_{pt}}} \tag{2.30}$$

2.2.6 Nozzles

Nozzles have as main function accelerating the gas coming from the fan, bypass nozzle, or the turbine, exhaust nozzle, expelling it at high velocity from the engine to provide thrust. Nozzles can be either convergent nozzles or convergent-divergent nozzles, being the first usually used on engines for subsonic aircraft and the second on engines for supersonic aircraft. It will only be modeled convergent nozzles, as the engine in study is mainly for civil aircraft applications under subsonic flight.

Bypass Nozzle Model

The nozzle can be assumed adiabatic, so the stagnation temperature is assumed constant along the nozzle.

$$T_{t8} = T_{t3} \tag{2.31}$$

The bypass nozzle can be either chocked, with $M_8 = 1$, or non chocked, with $M_8 < 1$, depending on the pressure gradient through the nozzle. It can then be defined a pressure ratio where $M_8 = 1$ and the pressure at the exit of the nozzle is critical, P_{8c}:

$$\frac{T_{t8c}}{T_{8c}} = \frac{T_{t3}}{T_{8c}} = \left(1 + \frac{\gamma - 1}{2} M_8^2\right) = \frac{\gamma + 1}{2} \tag{2.32}$$

$$\frac{P_{t3}}{P_{8c}} = \left(\frac{T_{t3}}{T_{8cs}}\right)^{\left(\frac{\gamma}{\gamma-1}\right)} = \frac{1}{\left[1 - \frac{1}{\eta_n}\left(1 - \frac{2}{\gamma+1}\right)\right]^{\frac{\gamma}{\gamma-1}}} \tag{2.33}$$

If the critical pressure is less than the ambient pressure, then the pressure at the exit of the nozzle is the ambient pressure and $M_8 < 1$.

Core or Exhaust Nozzle Model

Like the bypass nozzle, it can also be assumed adiabatic and it can also be defined a critical pressure ratio of the core nozzle:

$$T_{te} = T_{t7} \tag{2.34}$$

$$\frac{T_{tec}}{T_{ec}} = \frac{T_{t7}}{T_{ec}} = \left(1 + \frac{\gamma_g - 1}{2} M_e^2\right) = \frac{\gamma_g + 1}{2} \tag{2.35}$$

$$\frac{P_{t7}}{P_{ec}} = \left(\frac{T_{t7}}{T_{ecs}}\right)^{\left(\frac{\gamma_g}{\gamma_g-1}\right)} = \frac{1}{\left[1 - \frac{1}{\eta_n}\left(1 - \frac{2}{\gamma_g+1}\right)\right]^{\frac{\gamma_g}{\gamma_g-1}}} \tag{2.36}$$

then:

$$\frac{P_{t7}}{P_{ec}} > \frac{P_{t7}}{P_0}, \text{ non choked and } M_e < 1$$
$$\frac{P_{t7}}{P_{ec}} \leq \frac{P_{t7}}{P_0}, \text{ choked and } M_e = 1$$

2.2.7 Specific Thrust and Thrust Specific Fuel Consumption

The engine designed specific thrust, Ψ is calculated by the sum of the specific thrust generated by the bypass and core flow. Considering the proprieties of the gases exiting the nozzles, the respective

specific thrusts, and net specific thrust can be computed as follows:

$$\Psi = \frac{T_{bypass}}{\dot{m}g} + \frac{T_{core}}{\dot{m}g} \tag{2.37}$$

$$\frac{T_{bypass}}{\dot{m}g} = \frac{\dot{m}_b(u_8 - u_0)}{\dot{m}g} + \frac{A_8(p_8 - p_0)}{\dot{m}g} \tag{2.38}$$

$$\frac{T_{core}}{\dot{m}g} = \frac{\dot{m}_c(u_e - u_0)}{\dot{m}g} + \frac{A_e(p_e - p_0)}{\dot{m}g} \tag{2.39}$$

where

$$u_8 = M_8\sqrt{\gamma R T_8} \tag{2.40}$$

$$u_e = M_e\sqrt{\gamma R T_e} \tag{2.41}$$

and where the unknown areas of the exit nozzles and mass flows are resolved by the following relationships:

$$\dot{m}_{bypass} = \rho_8 u_8 A_8, \quad \rho_8 = \frac{p_8}{RT_8}, \quad \frac{\dot{m}_{bypass}}{\dot{m}} = \frac{B}{B+1}$$

$$\dot{m}_{core} = \rho_e u_e A_e, \quad \rho_e = \frac{p_e}{RT_e}, \quad \frac{\dot{m}_{core}}{\dot{m}} = \frac{1}{B+1}$$

The specific fuel consumption, SFC, can be obtained by the following expression:

$$SFC = \frac{\dot{m}_f g}{T_N} \tag{2.42}$$

Using equation (2.21) the specific fuel consumption can be related with the specific thrust as follows:

$$SFC = \frac{1}{B+1}\frac{1}{\Psi}\frac{c_{pg}T_{t5} - c_p T_{T_{t4}}}{\eta_b HV_{fuel} - c_{pg}T_{t5}} \tag{2.43}$$

2.3 Model Results and Validation

In this section the proposed thermodynamic model of the turbofan is validated by comparing the achieved results with those obtained using the GasTurb® software [47]. The turbofan performance is analyzed through the computation of the Specific Thrust, ψ, and Specific Fuel Consumption, SFC, with the variation of the following design parameters around their baseline values: Bypass ratio, Fan Pressure Ratio, Compressor Pressure Ratio and Turbine Inlet Temperature. Unless when shown otherwise, design parameters throughout the analysis will figure the baseline values proposed by GasTurb® manual [47], as listed below:

Baseline:

$$B = 5$$
$$FPR = 1.6$$
$$CPR = 18.75$$
$$TIT = 1600K$$

Regarding the real engine cycle analysis, the efficiencies and pressure drops in the various components are considered constant throughout the analysis. The values of the efficiencies and pressure drops are listed below:

$$\pi_d = 0.95 \qquad \eta_b = 0.95$$
$$\eta_{pf} = 0.85 \qquad \pi_b = 0.95$$
$$\eta_{pc} = 0.85 \qquad \eta_{pn} = 0.999$$
$$\eta_{pt} = 0.85 \qquad \eta_m = 0.999$$

The thermodynamic proprieties of air and fuel are also considered constant throughout the analysis and their values are expressed as follows:

$$HV_{fuel} = 43.4\ kJ/kg$$
$$\gamma = 1.4$$
$$\gamma_g = 1.33$$
$$c_p = 1005\ J/(kgK)$$
$$c_{pg} = 1140\ J/(kgK)$$

The analysis was carried out for a design point at an operating altitude of $h = 10000m$, and a flight Mach number of $M_0 = 0.8$.

2.3.1 Turbofan Performance vs Bypass Ratio

The performance parameters, Ψ and SFC, were computed ranging the bypass ratio from 1 to 10, yielding the following results.

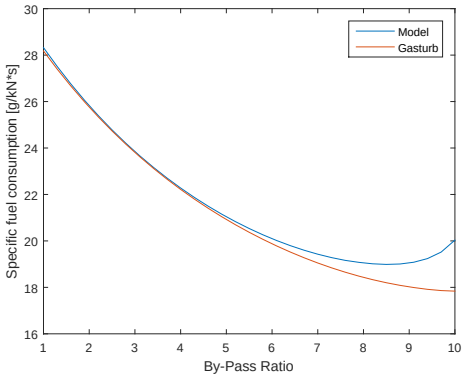

Figure 2.2: Specific Fuel Consumption versus By-pass Ratio.

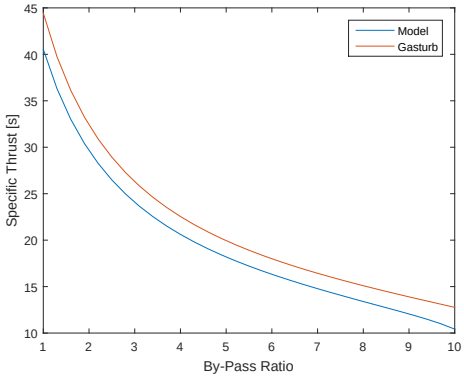

Figure 2.3: Specific Thrust versus Bypass Ratio.

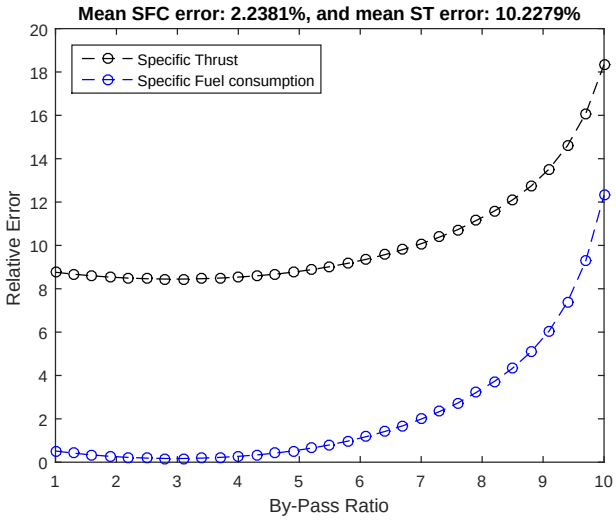

Figure 2.4: SFC and Ψ Relative Error variation.

The obtained values from both the proposed model and the GasTurb® software, show good agreement in the computed performance parameters for the evaluated bypass ratios. The computed SFC present a mean relative error of 2.2%, while the computed Ψ present a mean relative error of 10.2%. It is also worth noting the increase of the error presented at higher values of bypass ratio, this tends to happen as at high bypass ratios the calculus of performance parameters tend to be more sensible and thus may vary from the GasTurb® approach.

2.3.2 Turbofan Performance vs Fan Pressure Ratio

In this design point analysis, the performance parameters were computed throughout different fan pressure ratios, ranging from 1 to 2.5,

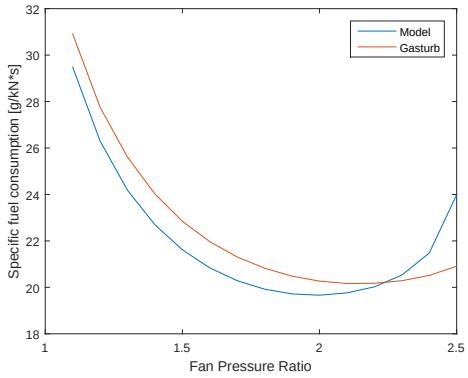

Figure 2.5: Specific Fuel Consumption versus Fan Pressure Ratio.

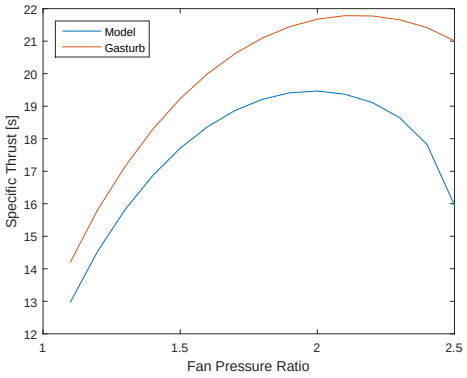

Figure 2.6: Specific Thrust versus Fan Pressure Ratio.

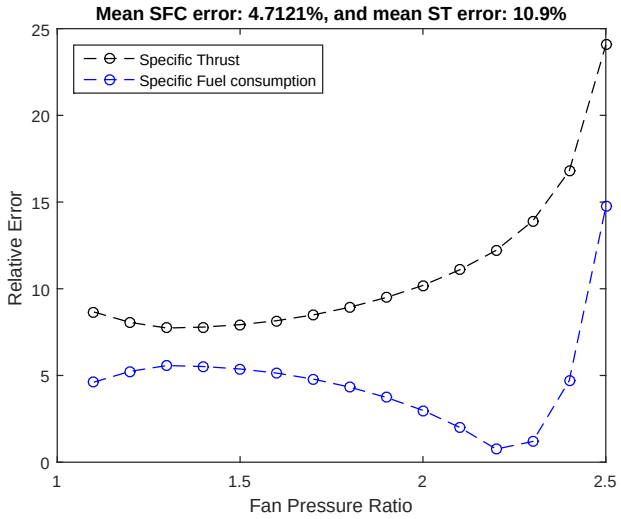

Figure 2.7: SFC and Ψ Relative Error variation.

The computed values present a good agreement with the results obtained from the GasTurb® software for the presented range of FPR. The SFC yields a relative mean error of 4.7% and the Ψ yields a mean relative error of 10.9%. The decrease in relative error towards Fan pressure ratios of 2.25 is justified by the crossing of lines experienced at figure 2.5.

2.3.3 Turbofan Performance vs Compressor Pressure Ratio

In this section, the turbofan performance parameters were computed for a different compressor pressure ratios, ranging from 3 to 40.

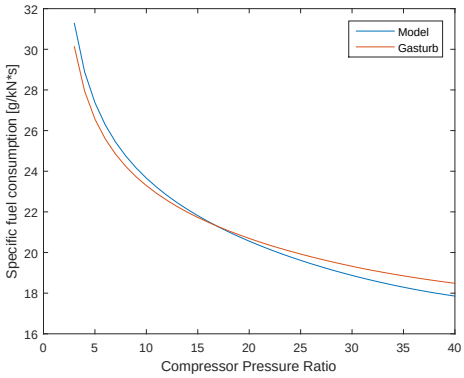

Figure 2.8: Specific Fuel Consumption versus Compressor Pressure Ratio.

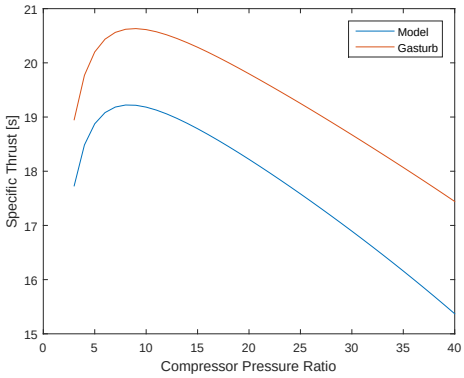

Figure 2.9: Specific Thrust versus Compressor Pressure Ratio.

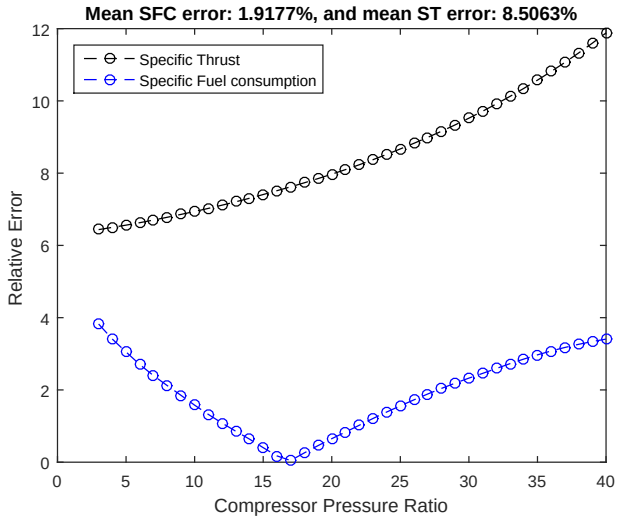

Figure 2.10: SFC and Ψ Relative Error variation.

A good agreement was obtained between both computed values for the range of compressor pressure ratios. The mean relative error for the SFC and Ψ were, respectively, 1.9% and 8.5%. The decrease in relative error towards Compressor pressure ratios of 16 is justified by the crossing of lines experienced at figure 2.8.

2.3.4 Turbofan Performance vs Turbine Inlet Temperature

For the last set of values, performance parameters were computed for various values of turbine inlet temperature, ranging from 1300K to 2000K.

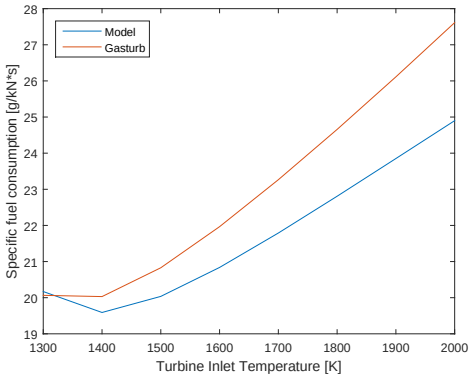

Figure 2.11: Specific Fuel Consumption versus Turbine Inlet Temperature.

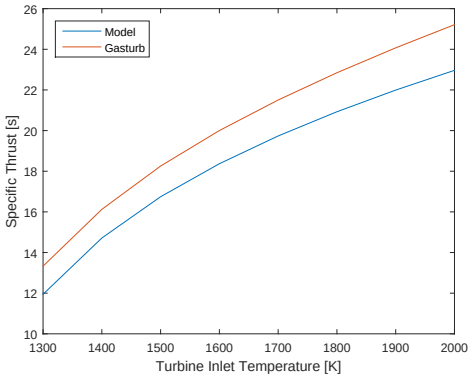

Figure 2.12: Specific Thrust versus Turbine Inlet Temperature.

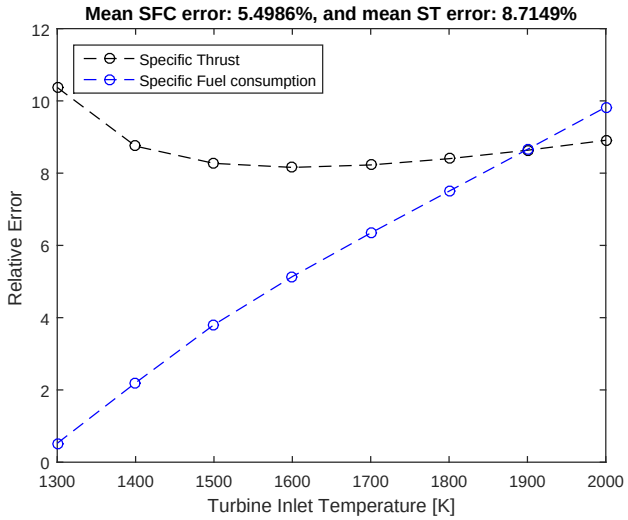

Figure 2.13: SFC and Ψ Relative Error variation.

The obtained results from both the proposed model and the GasTurb® software achieve a good agreement within the range of computed turbine inlet temperature values. The computed performance parameters present a mean relative error of 5.5% for the SFC and 8.7% for Ψ.

It is worth noting that the mean relative error is inferior in all the cases presented for the computation of SFC when comparing with the computations of Ψ.

2.4 Model Results vs ICAO Data

In this section, the proposed turbofan model performs the computation of the specific fuel consumption using the inputs retrieved from the ICAO Data Bank [48]. Such inputs are the overall compression ratio, bypass ratio and date when first tested. In this case, the results were computed using the data of the two-spool engines from General Electric engines only, thus providing the necessary consistency of manufacturer design preferences. Under the limitation of the design data available, the fan pressure ratio is assumed to be 1.7 throughout the analysis. This analysis refer for take-off conditions, with $M_0 = 0$ and $H = 0m$. To compute the specific fuel consumption, the fuel mass flow, $\dot{m}_f$, and engine maximum thrust, T_N, relative to take-off conditions are retrieved from the data from ICAO data bank, and equation (2.42) is directly applied.

In order to accommodate the technological advancements made throughout the years, it is defined four levels of technology regarding component efficiencies, pressure drops and thermal resistance [46]. These levels of technology can be thought of as representing the technical capability for 20-yr increments in time, starting from 1945. Thus level 4 of technology presents typical component design values for the most recent manufactured engines for the time period 2005-2025. Table 2.1 provide the values for the different tech levels.

Table 2.1: Variation of component efficiencies, total pressure ratios, and temperature limits over the years.

Component	Figure of merit	Tech level 1	Tech level 2	Tech level 3	Tech level 4
Diffuser	π_{dmax}	0.9	0.95	0.98	0.995
Compressor	η_{pc}	0.8	0.84	0.88	0.9
Fan	η_{pf}	0.78	0.82	0.86	0.89
Combustor	π_b	0.9	0.92	0.94	0.95
	η_b	0.85	0.91	0.98	0.99
Turbine	η_{pt}	0.8	0.85	0.89	0.9
Nozzles	η_n	0.95	0.97	0.98	0.995
Mechanical shaft	η_m	0.95	0.97	0.99	0.995
Maximum TIT [K]	T_{t5}	1100	1390	1780	2000

The thermodynamic proprieties of air and fuel are assumed constant and refer to the values used in the analysis made in section 2.3. The proposed turbofan model produced the results expressed in figure 2.14.

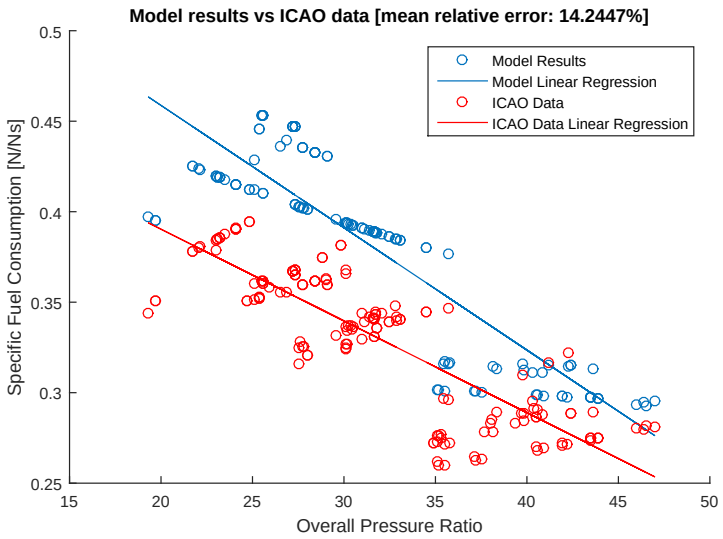

Figure 2.14: Turbofan model vs ICAO data: SFC as function of overall pressure ratio.

Considering the limited information provided for the conducted analysis, the proposed model proves to yield reasonable results throughout the range of engines analyzed. As can be denoted, the proposed model tends to over estimate the specific fuel consumption, although relative error decrease with the increase of the overall pressure ratio, achieving good correlation towards the high pressure ratios zone. The mean relative error of 14.2% proves a reasonable correlation with the real data. It is also important to denote that the underestimation presented when the results were compared with those of GasTurb® software was not of great importance as the proposed model actually tends to slightly over estimate the results when faced with real data.

3

Combustion Model

Contents

In this chapter it will be presented the process of the formulation of the primary zone combustion model as well as its validation process.

3.1 Hydrocarbon Combustion

Since the beginning of commercial aviation in the 1950's, the hydrocarbons used as a fuel in aviation gas turbine applications are the kerosene-type fuels, Jet-A or Jet-A1. These fuels present to be the norm around the world, with exception of Commonwealth of Independent States (CIS) and some parts of eastern Europe which use TS-1, a light kerosene-type of fuel. In the present work will be used a kerosene-type of fuel with composition CH_m, where m denotes the hydrogen to carbon ratio.

3.1.1 Combustion Stoichiometry

The combustion process is characterized by fast oxidation of, in this case, a hydrocarbon fuel which leads to a high release of thermal energy. The oxidizer, in this case the air, which is composed of oxygen, nitrogen, and small amounts of argon and carbon dioxide and other traces species like neon, helium and methane. Throughout this work the atmospheric air will be defined by its two major constituents, 20.9% of O_2 and 79.1% of N_2 in mole basis. Thus for every mole of O_2 required for combustion, 3.78 moles of N_2 must be accounted as well.

As been denoted in chapter 1, nitrogen is of major importance as it impacts on the thermodynamics, chemical kinetics, and the formation of pollutants in combustion systems. It is also important to denote that very few combustion systems can operate at stoichiometric conditions for the reason that such level of prefect level of mixing between fuel and air is impracticably attained. For this matter, in order to normalize the fuel to air ratio, which define the operating conditions of a combustor, it is used the stoichiometric fuel to air ratio resulting in the equivalence ratio, Φ, defined by:

$$\Phi = \frac{m_f/m_a}{(m_f/m_a)_s} \tag{3.1}$$

The combustion stoichiometry for a hydrocarbon fuel can then be written in the following form:

$$CH_m + \frac{\alpha_s}{\Phi}(O_2 + 3.78N_2) \longrightarrow CO_2 + \frac{m}{2}H_2O + \alpha_s\left(\frac{1}{\Phi} - 1\right)O_2 + \frac{3.78\alpha_s}{\Phi}N_2 \tag{3.2}$$

where $\alpha_s = 1 + m/4$.

3.1.2 Combustion Thermodynamics

The fast release of energy achieved through the chemical reaction lead to a substantial increase of the combustion gases temperature, reaching as high as 2500 K for the applications in study. In order to evaluate the formation of the products of combustion and pollutants, at such high temperatures, one must evaluate the chemical potential of combustion through an energy balance across the combustor.

First Law of Thermodynamics

A careful energy analysis through the first law of thermodynamics can provide good estimates of flame temperature needed to assess the combustion process itself and to calculate the concentration of the resulting chemical species. The first law states that in a closed system of fixed mass and identity, the change in total energy is equal to the heat exchange between the system and its surroundings minus the work done by the system on its surroundings.

$$dE = \delta Q - \delta W \tag{3.3}$$

In the case of a combustor the first law has to be rewritten for a control volume rather than a fixed mass, in order to accommodate the entrance and exit of combustion species through the boundaries of the system. In this case the energy equation takes the following form:

$$\frac{dE}{dt} + \sum_{j,out}(\bar{e}_j + p\bar{v}_j)\bar{f}_j - \sum_{i,in}(\bar{e}_i + p\bar{v}_i)\bar{f}_i = Q - W_x \tag{3.4}$$

where $\bar{e}$ denotes the mass specific energy, $\bar{v}$ the mass specific volume, $\bar{f}_i$ and $\bar{f}_j$ the mass flow rates entering and leaving the control volume respectively, Q the rate of heat transfer and W_x the rate at which work is done in the surroundings by the system. For the system in consideration, the kinetic and potential energy terms of the total energy system can be neglected, therefore the energy equation can be expressed in terms of the internal energy and on a molar basis.

$$\frac{du}{dt} + \sum_{j,out} f_j h_j - \sum_{i,in} f_i h_i = Q - W_x \tag{3.5}$$

where $h = u + pv$ denotes the molar specific enthalpy, which can then be define and evaluated with respect to the chemical reference state, usually at $T_0 = 298k$ and $p_0 = 1atm = 101kPa$, under the expression (3.6).

$$h_i^\circ(T) = h_i(T) - h_i(T_0) + \Delta h_{fi}^\circ(T_0) \tag{3.6}$$

where $\Delta h_{fi}^\circ(T_0)$ denotes the enthalpy of formation and the sensible enthalpy term, $h_i(T) - h_i(T_0)$, can be obtained by integrating the specific heat at constant pressure over the temperature.

$$h_i(T) - h_i(T_0) = \int_{T_0}^{T} c_{p,i}(T')dT' \tag{3.7}$$

The expression for the first law of thermodynamics for a chemically reacting open system can ultimately be written as

$$\frac{du}{dt} + \sum_{j,out} f_j[h_j(T) - h_j(T_0) + \Delta h_{fj}^\circ(T_0)] - \sum_{i,in} f_i[h_i(T) - h_i(T_0) + \Delta h_{fi}^\circ(T_0)] = Q - W_x \tag{3.8}$$

Dissociation and Chemical Equilibrium

In reacting systems where the products temperature reach below 1250 K, it is usually a good approximation to assume that the combustion products are the fully oxidized and stable species, CO_2, H_2O and N_2, and even O_2 in case of fuel-lean conditions [49]. Although this is not the case in the most combustion systems, which in this particularly application can reach as high as 2500 K as noted before.

At such high temperatures, chemical species that were stable can dissociate leading to the formation of other species and removing energy from the reaction throughout the dissociation process. For this reason, reduced species can be present in the final products of combustion even if sufficient oxygen is present for complete combustion. These species are continuously oxidized and replenished by dissociation and other reaction that occur in the hot gases. The concentration for those species are defined by the balance between the reactions of formation and consumption.

In order to determine the concentration of these species at high temperatures, a chemical equilibrium approach provides a good first approximation. Chemical equilibrium conditions are derived from the second law of thermodynamics and can be stated in term of Gibbs free energy, $G = H - TS$ [50]. Through the analysis of Gibbs free energy it can be defined an equilibrium constant, at constant pressure, for each reaction in consideration [51].

$$K_p(T) \equiv exp\left(- \frac{\sum_j v_j \mu_j^\circ}{RT} \right) = \prod_{j,\text{gas only}} (y_j p)^{v_j} \tag{3.9}$$

where μ_j° is the partial molar Gibbs free energy at the reference pressure, $p_0 = 1atm$, or standard chemical potential, v_j is the stoichiometric coefficient and f_j is the mole fraction of the species j. μ_j° is defined as follows:

$$\mu_j^\circ = \mu_j = h_j - Ts_j \tag{3.10}$$

where s_j is the partial molar entropy of species j, and is defined by the following expression:

$$s_j = s_j^\circ(T_0) + \int_{T_0}^{T} \frac{c_{p,j}(T')}{T'} dT' \tag{3.11}$$

where s_j° is the entropy at the reference state.

3.1.3 Combustion Kinetics

Equilibrium concentrations of the reaction products can be determined by the chemical equilibrium analysis, provided that the system maintains its pressure and temperature for a sufficiently long time. However, chemical reactions advance at finite rates, therefore equilibrium is not attained instantaneously. For this reason, finite rates of reaction allow the concentration of pollutants to largely vary from its equilibrium concentration.

In order to reduce pollutants like NO, which have their formation peak close to $\Phi = 1$, the equivalence ratio could be reduced to values below 0.5. However, reducing the equivalence ratio to this levels would also reduce the rate of the combustion reaction by lowering the temperature of reaction, leading to a weakening of the hydrocarbon oxidation and ultimately resulting in the reaction to cease

to continue within the flammability limits, reaching the so-called Lean Blow-Out. Since the residence time in combustor systems is also limited, reducing the combustion rate in order to minimize the pollutant formation would lead to the escape of partially reacted hydrocarbons and carbon monoxide.

Therefore, to understand the chemical factors that control pollutant formation, it is necessary to carefully examine the rate at which the combustion system achieve the final equilibrium state. Also, to define the rate at which chemical equilibrium is to be approached, it is necessary to assess the rates of reaction of each reaction present in the overall reaction mechanism.

3.2 NO_x formation mechanisms

As stated before, NO_x is the general name given to both NO and NO_2, since the majority of the produced NO_x are emitted as NO. The nitric oxide molecule is converted in NO_2 by reacting with atmospheric oxygen when in contact with the atmospheric air at the exhaust .

NO_x formation is usually defined by the thermal fixation of atmospheric nitrogen, Thermal NO_x; by the reaction of atmospheric nitrogen with a free hydrocarbon radical, Prompt NO; by organically bound nitrogen, present in certain fuels, which is readily oxidized, Fuel NO_x; or by reacting with N_2O which is formed in at high pressure conditions, N_2O pathway. Fuel NO_x are most relevant, and the predominant source of NO_x formation, when burning fuels with bounded nitrogen, as in the case of coal. Prompt NO_x formation occurs at low temperature, fuel-rich conditions and short residence times. Fuel NO_x and Prompt NO_x are not going to be assessed in this work, since their contribution proved to be negligible at the conditions of this study, which focus on fuel-lean conditions at high temperature and pressure where the fuel burnt don't have any bounded nitrogen. Thermal and N_2O pathways will be discuss in the following sections 3.2.1 and 3.2.2, respectively, as at high temperatures and pressures conditions they represent the major contributors for NO_x emissions.

3.2.1 Thermal NO_x

Thermal NO_x derive from the thermal fixation of atmospheric nitrogen through the overall oxidation reaction expressed below:

$$\frac{1}{2}N_2 + \frac{1}{2}O_2 \rightleftharpoons NO \tag{3.12}$$

This reaction is highly endothermic [$\Delta h_r^{\circ}(298) = 90.0 \quad KJmol^{-1}$], thus resulting that chemical equilibrium is just attained at very high temperatures present at near stoichiometric combustion. When temperatures are not sufficiently high the equilibrium concentration of NO decreases rapidly since its exponentially dependent of the temperature. The direct reaction of nitrogen with oxygen is to slow to be accounted for NO formation, however free oxygen atoms from O_2 dissociation or radical attack on O_2 are present and react readily with the N_2 molecules thus beginning a chain reaction mechanism, first postulated by Zeldovich in 1947 , and thus called the extended Zeldovich mechanism.

$$1) \qquad N_2 + O \rightleftharpoons NO + N \tag{3.13}$$

$$2) \qquad N + O_2 \rightleftharpoons NO + O \tag{3.14}$$

$$3) \qquad N + OH \rightleftharpoons NO + H \tag{3.15}$$

Reaction 2 presents to be more important than reaction 3 in fuel-lean conditions since the abundance of O_2 provides the sink for N.

In order to analyze the rate of formation of NO, combustion kinetics have to be applied to the complete combustion mechanism. The rate of formation of NO and N can be expressed in terms the concentrations of constituent species of the mechanism as follows.

$$R_{NO} = k_{+1}[N_2][O] - k_{-1}[N][NO] + k_{+2}[N][O_2] - k_{-2}[NO][O] + k_{+3}[N][OH] - k_{-3}[NO][H] \tag{3.16}$$

$$R_N = k_{+1}[N_2][O] - k_{-1}[N][NO] - k_{+2}[N][O_2] + k_{-2}[NO][O] - k_{+3}[N][OH] + k_{-3}[NO][H] \tag{3.17}$$

Rate constants for the Zeldovich mechanism are given by Hanson and Salimian [52] and are the following for the forward reactions:

$$k_{+1} = 1.8 \times 10^8 exp\left(\frac{-38370}{T}\right) \quad m^3 mol^{-1} s^{-1} \tag{3.18a}$$

$$k_{+2} = 1.8 \times 10^4 T exp\left(\frac{-4680}{T}\right) \quad m^3 mol^{-1} s^{-1} \tag{3.18b}$$

$$k_{+3} = 7.1 \times 10^7 exp\left(\frac{-450}{T}\right) \quad m^3 mol^{-1} s^{-1} \tag{3.18c}$$

and for the backward reactions:

$$k_{-1} = 3.8 \times 10^7 exp\left(\frac{-425}{T}\right) \quad m^3 mol^{-1} s^{-1} \tag{3.19a}$$

$$k_{-2} = 3.8 \times 10^3 T exp\left(\frac{-20820}{T}\right) \quad m^3 mol^{-1} s^{-1} \tag{3.19b}$$

$$k_{-3} = 1.7 \times 10^8 exp\left(\frac{-24560}{T}\right) \quad m^3 mol^{-1} s^{-1} \tag{3.19c}$$

The breaking of the triple bond from N_2 results in a high activation energy in reaction 1, setting the rate-limit of the chain mechanism. For this matter, NO production proceeds at a slower pace than the combustion reaction mechanism and is highly dependent of the temperature. It can then be assumed that O, H and OH radicals are present at their equilibrium concentrations, since NO formation just takes place after combustion reactions are complete.

A simplification proposed by Lavoie et al. [53] allows for a one-way rate of reaction be expressed as follows:

$$R_1 = k_{+1}[N_2]_e[O]_e = k_{-1}[N]_e[NO]_e \tag{3.20a}$$

$$R_2 = k_{+2}[N]_e[O_2]_e = k_{-2}[NO]_e[O]_e \tag{3.20b}$$

$$R_3 = k_{+3}[N]_e[OH]_e = k_{-3}[NO]_e[H]_e \tag{3.20c}$$

The rate of formation of NO and N can then be expressed by:

$$R_{NO} = R_1 - R_1\alpha\beta + R_2\beta - R_2\alpha + R_3\beta - R_3\alpha \tag{3.21}$$

$$R_N = R_1 - R_1\alpha\beta - R_2\beta + R_2\alpha - R_3\beta + R_3\alpha \tag{3.22}$$

where α and β are the following dimensionless quantities:

$$\alpha = \frac{[NO]}{[NO]_e} \tag{3.23}$$

$$\beta = \frac{[N]}{[N]_e} \tag{3.24}$$

The rate at which NO is formed is dependent of the concentration of N. Since the activation energy for the nitrogen reaction with oxygen in reaction 2 is small and, in fuel-lean conditions, O_2 is in excess, an important assumption can be made by considering that the free atoms of N are readily consumed as they are formed by reaction 1, thus allowing to establish a quasi-steady state approach.

$$R_N = \frac{d[N]}{dt} = 0 \tag{3.25}$$

Equation (3.22) can then be equaled to zero and a dimensionless N concentration for the steady-state be defined as, β_{ss}:

$$\beta_{ss} = \frac{\kappa + \alpha}{\kappa\alpha + 1} \tag{3.26}$$

where κ is given by:

$$\kappa = \frac{R_1}{R_2 + R_3} \tag{3.27}$$

The rate of formation of NO can then be written in terms of α and known quantities as follows:

$$R_{NO} = \frac{d[NO]}{dt} = \frac{2R_1(1-\alpha^2)}{1+\kappa\alpha} \tag{3.28}$$

A differential equation for α is written for a constant pressure and temperature:

$$\frac{d\alpha}{dt} = \frac{1}{[NO]_e}\frac{2R_1(1-\alpha^2)}{1+\kappa\alpha} \tag{3.29}$$

This equation can now be integrated, assuming $[NO]_{t=0} = 0$, resulting in the following expression.

$$(1-\kappa)ln(1+\alpha) - (1+\kappa)ln(1-\alpha) = \frac{t}{t_{NO}} \tag{3.30}$$

In equation (3.30) the t_{NO} is the characteristic time for NO formation and is defined by:

$$t_{NO} = \frac{[NO]_e}{4R_1} \tag{3.31}$$

The characteristic time for NO formation represents the time necessary so that NO concentration would achieve equilibrium if the reaction would proceed at the initial rate.

The rate equation for N, the dimensionless N concentration and the characteristic time for N formation can also be written as follows:

$$[N]_e\frac{d\beta}{dt} = R_1 - (R_2 + R_3)\beta \tag{3.32}$$

$$\beta = \kappa\left[1 - exp\left(-\frac{t}{t_N}\right)\right] \tag{3.33}$$

$$t_N = \frac{[N]_e}{R_2 + R_3} \tag{3.34}$$

Analyzing the characteristic time for N formation when compared with characteristic time for NO formation, the assumption of a quasi-steady state can be readily validated, since the t_{NO} is several orders of magnitude larger than t_N for adiabatic combustion throughout the range of temperatures where the Zeldovich mechanism for the formation of NO is relevant [54]. [see table A.1 at Annex A.1].

3.2.2 N_2O Pathway

The N_2O pathway for NO_x formation is usually associated to fuel-bound nitrogen. However, studies [55][56] suggest a relevant contribution of the nitrous oxide pathway in combustion systems with high pressure and lean-fuel conditions, contributing about 15% to total NO_x formation. Also, as stated in chapter 1.1, N_2O emissions represent major importance concerning the environment, since its elevated GWP.

Assuming the absence of fuel-bound nitrogen and its influence in the production of nitrous oxide, a reaction mechanism can be define for the N_2O pathway as follows.

$$N_2O + M \rightleftharpoons N_2 + O + M \tag{3.35}$$

$$N_2O + O \rightleftharpoons NO + NO \tag{3.36}$$

$$N_2O + H \rightleftharpoons NO + NH \tag{3.37}$$

$$N_2O + H \rightleftharpoons N_2 + OH \tag{3.38}$$

$$N_2O + O \rightleftharpoons N_2 + O_2 \tag{3.39}$$

$$N_2O + OH \rightleftharpoons N_2 + HO_2 \tag{3.40}$$

$$N_2O + OH \rightleftharpoons NH + NO_2 \tag{3.41}$$

$$N_2O + OH \rightleftharpoons NO + HNO \tag{3.42}$$

$$N_2OH_2O \rightleftharpoons NH_2 + NO_2 \tag{3.43}$$

$$N_2OH_2O \rightleftharpoons HNO + HNO \tag{3.44}$$

$$N_2O + CO \rightleftharpoons NCO + NO \tag{3.45}$$

In order to simplify the the reaction mechanism some assumptions can be made with the respective physical justification. Since NH is just present in trace concentration, the reverse reaction in (3.37) occurs to a very small extent, thus allowing to be neglected. Analogously, the reverse reactions of (3.41) – (3.45) can also be neglected since HNO, NH_2 and NCO are also present in low concentrations.

3.3 Combustion Model Algorithm

Regarding NO_x emissions, a combustion model was formulated in order to achieve a comprehensive simulation of the reaction mechanism occurring inside a gas turbine combustor. Seeing that the thermal contribution through the Zeldovich reaction mechanism accounts for the majority of the NO_x formation, the proposed model uses the above-mentioned kinetic analysis of section 3.2.1 paired with the adiabatic temperature of combustion achieved through the combustion thermodynamics analysis made in 3.1.2. The contribution of the N_2O pathway is not formulated since its just represents 15% of total NO_x emissions [56], thus keeping the model less computationally demanding while not compromising the comprehensive analysis of the combustion reaction.

Considering the 0D approach of the combustion model, the reaction zone can be modeled taking into account the following inputs: the entry conditions of the pressurized air in the combustor, represented by the stagnation temperature and pressure after the compressor stage; the equivalence ratio, Φ; and the residence time in the reaction zone of the combustor.

The reaction mechanism proposed to combustion equilibrium is represented by the following reactions:

$$CO_2 \rightleftharpoons CO + \frac{1}{2}O_2 \tag{3.46}$$

$$H_2O \rightleftharpoons H_2 + \frac{1}{2}O_2 \tag{3.47}$$

$$\frac{1}{2}N_2 + \frac{1}{2}O_2 \rightleftharpoons NO \tag{3.48}$$

$$\frac{1}{2}N_2 \rightleftharpoons N \tag{3.49}$$

$$\frac{1}{2}O_2 \rightleftharpoons O \tag{3.50}$$

$$\frac{1}{2}H_2O + \frac{1}{4}O_2 \rightleftharpoons OH \tag{3.51}$$

$$\frac{1}{2}H_2O \rightleftharpoons H + \frac{1}{4}O_2 \tag{3.52}$$

The following assumptions were already mentioned but are again refereed in order to highlight the model restrictions:

1. The reaction zone is adiabatic.
2. O, H and OH radicals are present at their equilibrium concentrations.
3. N rate of formation is considered to be in a quasi-steady state.
4. The NO formation takes place after the combustion reaction at constant adiabatic temperature of combustion and is bellow equilibrium.

With the above assumptions made the following algorithm was elaborated to compute the formation of NO through the paired equilibrium and kinetic analysis:

1. Set the input conditions at the inlet of the combustor, T_0, p, Φ and t_r.
2. Define adiabatic combustion equilibrium reaction stoichiometry.

$$CH_m + \frac{\alpha_s}{\Phi}(O_2 + 3.78N_2) \longrightarrow n_{CO_2}CO_2 + n_{H_2O}H_2O + \\ + n_{O_2}O_2 + n_{N_2}N_2 + n_{CO}CO + n_{H_2}H_2 \tag{3.53}$$

   where the stoichiometry coefficient of the products of combustion are given by the equilibrium relationship of the reactions 3.46 – 3.52.

3. Estimate a value for adiabatic temperature of combustion Tad.

4. Define the equilibrium constants for each equilibrium reactions in function of the estimated temperature, T_{ad}.

$$K_{p,i}(T) = exp\left(- \frac{\sum_j v_{ji}\mu_j^\circ}{RT} \right) = \prod_{j,\text{gas only}} (y_j p)^{v_j} \tag{3.54}$$

where v_{ji} denotes the stoichiometric coefficient for species j in reaction i and μ_j° the chemical potential of species j and is defined by:

$$\mu_j^\circ = \int_{T_0}^{T} c_{p,i}(T')dT' + \Delta h_{fj}^\circ(T_0) - T\left[s_j^\circ(T_0) + \int_{T_0}^{T} \frac{c_{p,j}(T')}{T'} dT' \right] \tag{3.55}$$

5. Define the equilibrium constants for each equilibrium reactions in function of equilibrium mole fractions.

$$K'_{p,i} = \prod_{j,\text{gas only}} (y_j p)^{v_j} \tag{3.56}$$

6. Solve the following non-linear system of equations retrieving the stoichiometric coefficient of the combustion products and define the respective mole fractions, y_j.

$$K_{e,i} = K_{p,i}(T) - K'_{p,i} = 0 \tag{3.57}$$

7. Define the energy equation.

$$F_T = \sum_{j,prod} v_j[h_j(T) - h_j(T_0) + \Delta h_{fj}^\circ(T_0)] - \sum_{i,react} v_i[h_i(T) - h_i(T_0) + \Delta h_{fi}^\circ(T_0)] \tag{3.58}$$

8. Solve the energy equation retrieving a new estimated temperature, T'_{ad}.

$$F_T = 0 \tag{3.59}$$

9. If the new estimated temperature is different than T_{ad}, then return to point 3 using the new estimated temperature as T_{ad} until $T_{ad} = T'_{ad}$.

10. Repeat steps 4 to 6 in order to retrieve the stoichiometric coefficient of the remaining species NO, N, O, OH and H in equilibrium conditions.

11. Define the reaction rates of the Zeldovich reaction mechanism using the equilibrium mole fractions.

$$R_1 = k_{+1}c^2 y_{N_2} y_{O_e} \tag{3.60a}$$

$$R_2 = k_{+2}c^2 y_{N_e} y_{O_2} \tag{3.60b}$$

$$R_3 = k_{+3}c^2 y_{N_e} y_{OH_e} \tag{3.60c}$$

12. Define characteristic time for NO, t_{NO}, and solve equation (3.30) for α.

13. Obtain the NO mole fraction.

$$y_{NO} = \alpha y_{NO_e} \tag{3.61}$$

As stated at section 3.2, the majority of the NO_x formed comes from the oxidation of the NO with the atmospheric oxygen at the exhaust. For this matter, the result of this algorithm, the mole fraction of NO, should suffice to give the reasonable predictions on NO_x emissions. In order to provide a more comprehensive and normalized way of analyzing the emissions level, a Emission Index (EI) is formulated [27]. The emission index for the specie i is given by the ratio of the mass flow rate of said specie and the mass flow rate of burnt fuel in the combustion process.

$$EI_i = \frac{\dot{m}_i}{\dot{m}_{fuel}} \tag{3.62}$$

This presents an important tool, as it readily reveals the the amount of pollutant emitted per mass of fuel, independently of dilution of exhaust or combustion efficiency of the system. In the present case of a hydrocarbon combustion the emission index can be expressed follows:

$$EI_i = \left(\frac{y_i}{y_{CO} + y_{CO_2}}\right)\left(\frac{nM_i}{M_f}\right) \times 10^3 \tag{3.63}$$

where M_i and M_f are the molecular weights of species i and fuel, respectively, while n represents the number of moles of carbon in a mole of hydrocarbon fuel. The ratio in the first brackets indicate the number of moles of species i per mole of carbon in fuel, as the ratio in the second brackets represent the conversion of carbon in fuel to mass units. It must then be multiplied by a thousand so it can be presented in the desirable units, g/kg of fuel.

3.4 Results and Model Validation

In order to validate the various steps taken in the formulation of this model, each main stage was submitted for validation. The results of the model are compared with reference values taken from [51].

Complete Combustion

The complete combustion process accounts for the combustion of a hydrocarbon and yields the mole fractions of products of the reaction, N_2, CO_2, H_2O and, when using excess air, O_2.

The first evaluated reaction, refers to the combustion of an heavy fuel oil with composition $CH_{1.8}$, at the atmospheric pressure and temperature, 1 atm and 298 K. Combustion takes place at stoichiometric conditions, $\Phi = 1$, and no error is presented for the mole fractions, since the results are calculated directly from stoichiometry.

Table 3.1: Comparison of results for a complete combustion of $CH_{1.8}$ at 1 atm and 298 K.

Evaluated Entities	Reference	Model	Relative Error
Mole fractions			
N_2	0.7425	0.7425	
CO_2	0.1355	0.1355	
H_2O	0.1220	0.1220	
Adiabatic Flame Temperature in K	2356.0	2355.5	0.02%

The second combustion reaction evaluated refers to the combustion of a aviation kerosene fuel with composition $CH_{1.88}$ and a lower heating value of 600 kJ (mol C)$^{-1}$ and burned with excess air

relative to stoichiometric conditions, $\Phi = 0.8$. The initial temperature and pressure of 560 K and 10 atm, respectively. The comparison of the reference values and the obtained results are expressed in the following table.

Table 3.2: Comparison of results for a complete combustion of $CH_{1.88}$ at 10 atm and 560 K.

Evaluated Entities	Reference	Model	Relative Error
Mole fractions			
N_2	0.7510	0.7506	0.05%
CO_2	0.1081	0.1081	0.00%
O_2	0.0397	0.0397	0.00%
H_2O	0.1020	0.1016	0.39%
Adiabatic Flame Temperature in K	2304.0	2306.4	-0.10%

From the expressed results in the above table, it can be stated that the model produces very accurate results with relative errors lower than 1% in both evaluated reactions.

Incomplete Combustion

In this second stage of validation, an incomplete combustion with dissociation products derived from combustion equilibrium is analyzed. The fuel used is the same heavy fuel oil, $CH_{1.8}$, under the same initial conditions, atmospheric pressure and temperature, 1 atm and 298 K. However, the dissociation reactions of CO_2 and H_2O, are now considered. In addition to the entities evaluated in the above validation, the mole fractions of CO and H_2 are also examined. Table 3.3

Table 3.3: Comparison of results for a incomplete combustion of $CH_{1.8}$ at 1 atm and 298 K.

Evaluated Entities	Reference	Model	Relative Error
Mole fractions			
N_2	0.7370	0.7375	-0.07%
CO_2	0.1230	0.0116	0.08%
O_2	0.00685	0.00690	-0.73%
H_2O	0.1190	0.1189	0.08%
CO	0.0115	0.0116	-0.87%
H_2	0.00217	0.00220	-1.38%
Adiabatic Flame Temperature in K	2261.0	2262.7	-0.001%

The model shows to validate well when faced with incomplete combustion, providing accurate estimates with relative errors inferior to 2%. Also, as expected, the adiabatic flame temperature decreases due to the endothermic dissociation reactions, representing a significant 10% difference when comparing to the first case for the same fuel in table 3.1. The model is also validated for the use of methane, CH_4, under atmospheric and stoichiometric conditions. [see Annex A.2].

Complete Combustion with thermal NO_x

For a validation of the full extend of the combustion model, the combustion kinetics are paired with combustion equilibrium, where the production of NO_x is evaluated through the production of NO in the Zeldovich mechanism. The combustion conditions are the same as the ones utilized in the validation of complete combustion. The equilibrium mole fractions of NO, N, O, OH and H are also compared

with the reference values alongside the NO mole fraction.

Table 3.4: Comparison of results for a complete combustion of $CH_{1.88}$ at 10 atm and 560 K with NO_x formation.

Evaluated Entities	Reference	Model	Relative Error
Mole fractions			
N_2	0.7510	0.7466	0.59%
CO_2	0.1081	0.1059	2.04%
O_2	0.0397	0.0398	-0.25%
H_2O	0.1020	0.1007	1.27%
NO_e	0.0072	0.0068	5.29%
N_e	1.04×10^{-8}	1.04×10^{-8}	-0.32%
O_e	3.01×10^{-4}	3.00×10^{-4}	0.33%
OH_e	2.58×10^{-3}	2.60×10^{-3}	-0.78%
H_e	5.47×10^{-5}	5.61×10^{-5}	-2.52%
NO	1.18×10^{-3}	1.15×10^{-3}	2.55%
Adiabatic Flame Temperature in K	2304.0	2306.4	-0.10%

As can be seen by the analysis of the above table, the model presents good results when pairing the equilibrium and kinetic analysis. Although the equilibrium concentrations where established, they were not accounted in the calculus of the adiabatic flame temperature. This was a choice made to simulate the same conditions as the ones expressed by the reference values and the approach taken by their author.

Incomplete Combustion with thermal NO_x

However, to simulate closer to real conditions, the equilibrium reactions responsible for dissociation of water and carbon dioxide must be accounted for the determination of the temperature of combustion. This is because, at the rate of a combustion reaction, the mentioned species do achieve equilibrium. Therefore, as mentioned before, since these dissociation reactions are highly endothermic, they end up removing a not negligible amount of energy to the combustion process.

In order to validate this conditions, the model pairs the dissociation processes of H_2O and CO_2 dissociation and the thermal formation of NO. The results are expressed in the table below where the relative error is replaced by the relative difference between values, as the model and reference values are just compared qualitatively instead of quantitatively, seen that they do not evaluate the same conditions.

Table 3.5: Comparison of results for a incomplete combustion of $CH_{1.88}$ at 10 atm and 560 K with NO_x formation.

Evaluated Entities	Reference	Model	Relative Difference
Mole fractions			
N_2	0.7510	0.7479	0.41%
CO_2	0.1081	0.1061	1.85%
O_2	0.0397	0.0405	-2.01%
H_2O	0.1020	0.1009	1.07%
CO		1.584×10^{-3}	
H_2		2.931×10^{-4}	
NO	1.180×10^{-3}	1.027×10^{-3}	12.98%
Adiabatic Flame Temperature in K	2304.0	2293.7	0.45%

The model results for the oxidation reaction with dissociation effects do not differ much from the former values in the four main combustion products, N_2, CO_2, O_2 and H_2O. As expected, the adiabatic flame temperature decreases. Even if small, the decrease in flame temperature by the endothermic dissociation reactions led to a significant decrease in NO formation. This proves the high sensibility of NO formation to variations of temperature, as mentioned before.

4

Thermo-Combustion Model

Contents

The current chapter serves to unify both turbofan, combustion and NO_x prediction models in order to compute and compare the results with real world conditions.

4.1 Combustion and Turbofan Model

In order to compute and optimize the design parameters in an early stage of a turbofan engine design, both turbofan and combustion process have been paired to give an overall understanding of the complete engine performance, regarding pollutant formation and specific fuel consumption.

Two models were assembled to produce estimates of the pollutant emission. The first unified model, pairs the turbofan model produced and validated at chapter 2 and the combustion model with dissociation effects and NO formation described and validated at chapter 3. The second unified model, consists in the turbofan model coupled with the NO_x emission prevision made through the expressions derived by Rizk $\&$ Mongia [34], which were already mentioned at chapter 1.

$$EI_{NO_x total} = EI_{NO_x pz} + EI_{NO_x ds} \tag{4.1a}$$

$$EI_{NO_x pz} = 10^{13}\left(\frac{p_{t3}}{1.4*10^6}\right)^{aa} exp\left(\frac{-71442}{T_{pz}}\right)(7.56\Phi^{-7.2} - 1.6)t^{0.64} \quad \text{g/kg fuel} \tag{4.1b}$$

$$EI_{NO_x ds} = 10^{14}\left(\frac{p_{t3}}{1.4*10^6}\right)^{aa} exp\left(\frac{-71442}{T_{pz}}\right)(1.172\Phi^{-4.56} - 0.6)t^{0.876} \quad \text{g/kg fuel} \tag{4.1c}$$

$$aa = 11.949 exp\left(-\frac{\Phi}{5.76}\right) - 10.0 \tag{4.1d}$$

For comparison purposes, the ICAO engine data bank will be used as source of the parametric inputs, such as overall pressure ratio, by-pass ratio and fuel composition, and also used to retrieve the the NO_x emission index to compare with the obtained results. The same set of engines selected in chapter 2.3, are also used now as reference.

Other conditions must also be taken into account so the values can be compared. For instance, as the reference values for EI_{NO_x} retrieved from the data bank refer to take-off conditions, the same conditions have to be applied to the models.

Some design parameters are susceptible to variation when applied to the models, such as the conditions at flame front in the primary zone of the combustor, namely equivalence ratio, Φ, and the residence time of the gases at combustion temperature, t_i. In the case of the model paired with Rizk $\&$ Mongia s expressions, the primary zone temperature, which is an explicit variable, is also susceptible to variation. As they are not expressed in the reviewed literature, since they are strongly correlated with the proprietary designs of the combustors, values for this entities are estimated and explained as follows.

The values for the equivalence ratio at the primary zone are assumed to be stoichiometric to simulated the takeoff conditions. This tends to corroborate with the semi-empirical approach of the Rizk $\&$ Mongia model, yielding good results. However, the more theoretical approach of the model developed in this thesis lead to an overestimation of the NO emissions when presented with $\Phi_{pz} = 1$. Therefore, the values for equivalence ratio considered to the developed combustion model, range from $\Phi_{pz} = 0.6$

to $\Phi_{pz} = 0.8$, in order to account for technological advancements made by the manufacturers to decrease NO_x emissions. The values for the residence time at flame front are also of great importance, therefore values of $t_i = 0.8ms$ to $t_i = 1ms$ are used as recommended by Odgers and Kretschmer's [40] and Flagan [51]. Lastly, the values for temperature variation in the primary zone range from $\Delta T_{pz} = 1500k$ to $\Delta T_{pz} = 1650k$, this values are then used in equation 4.2 in order to compute the primary zone temperature.

$$T_{pz} = T_{i,c} + \Delta T_{pz} \tag{4.2}$$

4.2 Model Results and Discussion

After the above mentioned considerations, a series of computations were made using input information from the available engine data bank. The information extracted was then compared to proceed with a comprehensive analysis.

4.2.1 Proposed Combustion Model

The first analysis is made using the proposed combustion model paired with the two-spool turbofan model. As previously explained, the values of Φ_{pz} and t_i are selected from the defined ranges. For the first set of engines the selected values are, $\Phi_{pz} = 0.7$ and $t_i = 1ms$. The results are presented in figure 4.1. The marked line defines the equality of the obtained results with the extracted results from the emissions data bank.

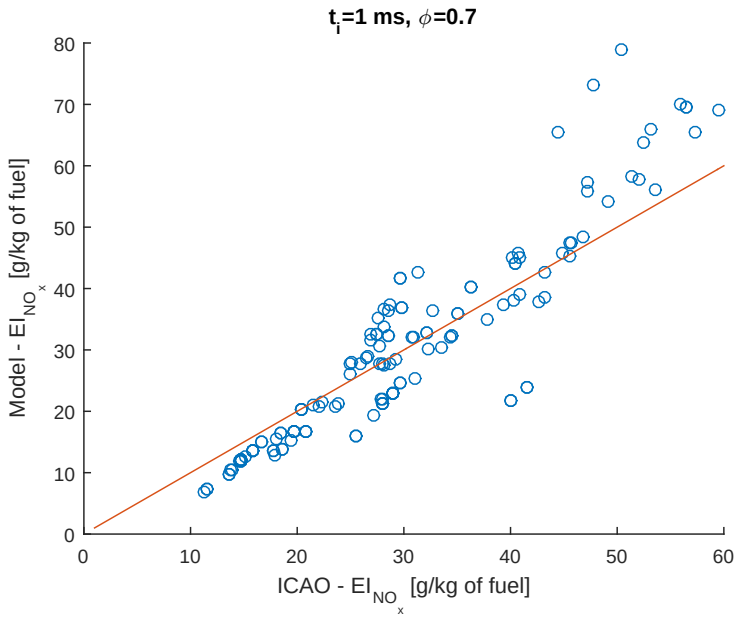

Figure 4.1: Results comparison with data from ICAO emissions data bank.

By analyzing the computation results, it can be show a good correlation for the majority of the compared values. However, for high compression ratios the model tend to over estimate. This happens, due to the exponential relation between the rate of NO formation and combustion temperature,

thus the high temperatures resulting from the high pressure compression ratios tend to be avoided by the manufacturers.

The proposed model is also compared with a second set of values which correspond to the next generation engines with state of the art combustor technology, the TAPS combustor. Therefore to accommodate the new technological paradigm, it is assumed that the primary zone accepts even leaner mixtures, thus reducing the NO formation rate. For this set of values a new par of primary zone parameter is then selected, $\Phi_{pz} = 0.65$ and $t_i = 0.8ms$.

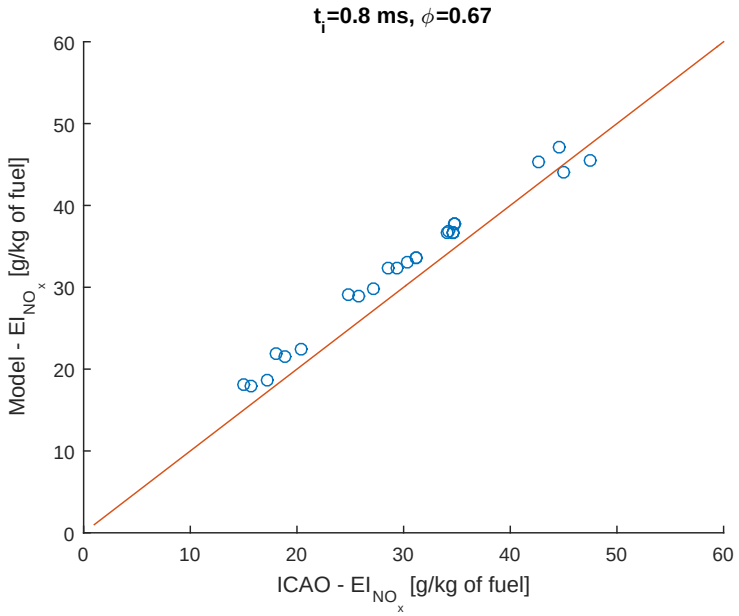

Figure 4.2: GEnx engines results comparison.

The obtained results are shown to be very favorable, with very good estimation throughout the wide range of compression ratios of the engines using this new combustor technology. Thus, proving to be a useful tool in an early-stage gas turbine engine design.

4.2.2 Rizk $\&$ Mongia Prediction Model

The second analysis focus upon the comparison of the Rizk $\&$ Mongia model paired with the turbofan model. As stated before, for this model is used the selected set of values, $\Phi_{pz} = 1$, $t_i = 1ms$ and a primary zone temperature variation, $\Delta T_{pz} = 1625k$.

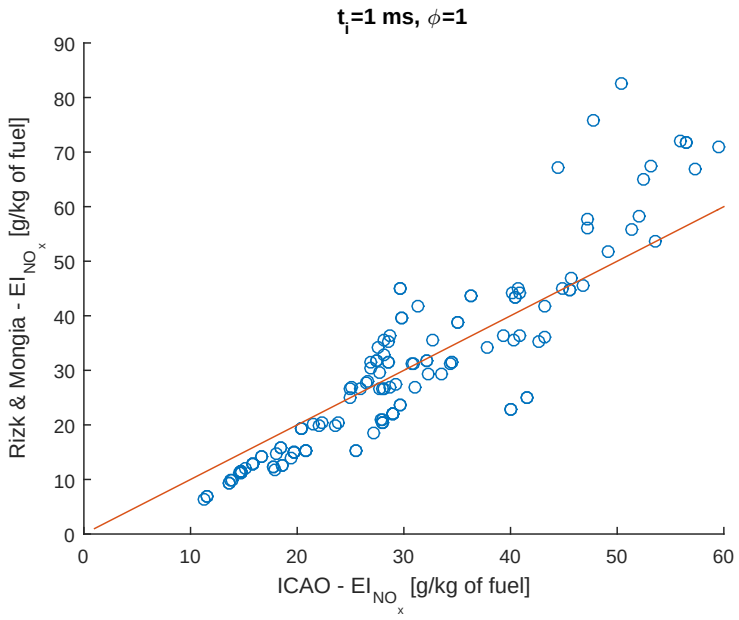

Figure 4.3: Rizk & Mongia results comparison.

The Rizk & Mongia model also provide a good estimation over the wide range of engines compared. As in the case of the proposed model, this model also tends to over estimate in the high compression region, which are justified as it were before. For the second set values of the GEnx engines, the Rizk & Mongia model also suffer from the alteration of the primary zone parameters. In this case the selected values are reduced, as they were for the model developed by this thesis, to $\Phi_{pz} = 0.91$ and $t_i = 0.8ms$, while maintaining $\Delta T_{pz} = 1625k$ from the former comparison. The results are expressed in the following figure.

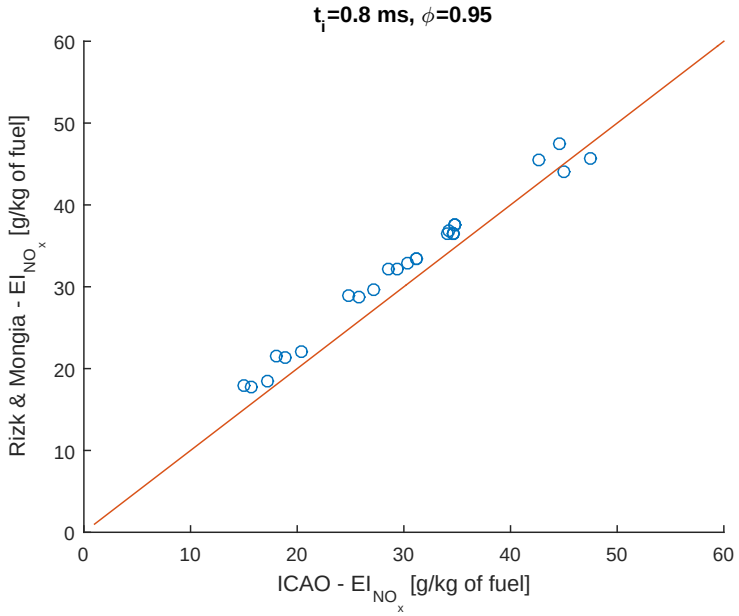

Figure 4.4: Rizk & Mongia, GEnx engines results comparison.

The results express a very good correlation with the extracted data of the GEnx engines.

It is important to compare the achieved temperatures for the primary zone in both models in order to analyze the consistence of both methods. This consistence can be verified in figure 4.5.

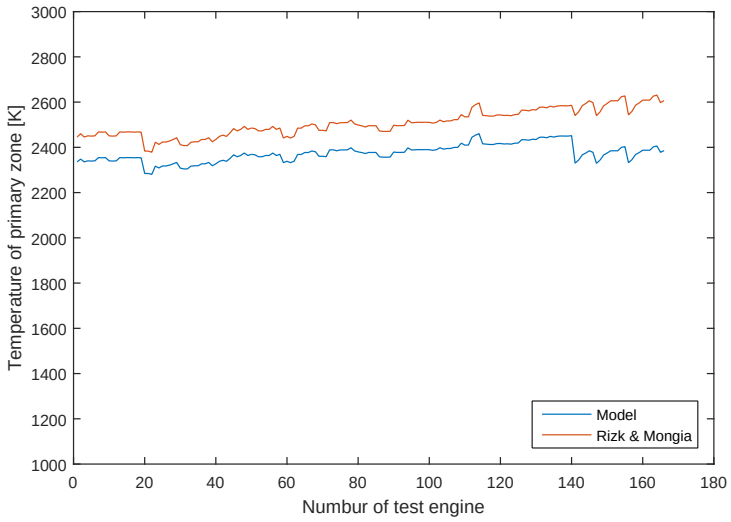

Figure 4.5: Primary Zone temperature of the Rizk $\&$ Mongia model versus proposed model.

As shown, the temperatures of both models, present small difference from each other, which provides coherence within the obtain results. This also corroborates with the choice of ΔT_{pz} for the Rizk $\&$ Mongia model, since the proposed model evaluate the combustion mechanism in detail. It is also important to note that the residence times are kept the same in the same sets of engines, also providing coherence throughout the analysis.

5

Optimization

Contents

The current chapter presents an optimization process resorting to genetic algorithms, in order to obtain the optimized design parameters in both single objective and multi objective conditions.

5.1 Optimization using Genetic Algorithms

One of the goals of the present work is to achieve optimized design parameters in order to minimize NO_x emissions within the range of current technology levels. To do so, a large number of variables have to be computed to find the optimal solution. It is also important to account that a single-objective oriented approach is not enough for the purpose of early stage design of a gas turbine. It is then also important to minimize fuel consumption while minimizing NO_x emissions, turning this optimization problem even more complex.

To address such problem it was selected Genetic Algorithms as a tool for the optimization process. These algorithms are based on the natural selection process that mimics biological evolution, where when given a random selection of initial parameters (i.e. individuals) the algorithm converges to the optimal solution of the objective function. The convergence is tackled through a series of cross-over and mutation of the individuals that result in a new set of values, called a new generation, until a set of optimal parameters is achieved. Genetic Algorithms are also favorable for this type of optimization problems as they converge to a global maximum or minimum better than the more classical derivative approach, and can handle constrained or unconstrained problem as well as Multi-Objective problems like the one present in this work. It is then needed to establish the objective functions, or fitness functions, and the set of parameters that are going to be varied in order to proceed with the algorithm.

Although a NO_x emissions model has been developed in Chapter 3, it proved to be too computationally expensive to use for optimization purposes. Instead it will be used the expressions derived from the model formulated by Rizk $\&$ Mongia [34], that were revised in Chapter 1, and were paired with the turbofan model in chapter 4. However, the proposed model will be used later, providing a more comprehensive analysis of the effects of the optimized parameters in the combustion process.

5.1.1 Single-Objective Optimization

As previously stated, the principal objective of the present work is to achieve a set of optimized parameters to minimize NO_x emissions and, for this matter, a Single-Objective optimization is set as a first approach. It is defined the following objective function:

$$EI_{NO_x total} = f(FPR, CPR, ti, \Phi) \tag{5.1}$$

Equation (5.1) denotes that NO_x emissions are a function of the pressure ratios in the compression stage and the combustor parameters, residence time t_i and equivalence ratio Φ. Other preliminary design parameters, like the Bypass ratio (B) and Turbine Inlet Temperature (TIT), were not included as the TIT is defined by the amount of dilution air after combustion and the Bypass ratio just defines the ratio between core and bypass streams, thus not influencing NO_x formation in the combustor. In order to compute the optimized values for this parameters, the constrain limits have been defined

within physically reasonable intervals and also accounting for future technological developments. The upper and lower limits are defined in the following table 5.1.

Table 5.1: Design Parameters limits.

Parameters	Lower limit	Upper limit
Fan Pressure Ratio (FPR)	1	2
Compressor Pressure Ratio (CPR)	10	40
Residence time in ms (t_i)	0.1	10
Equivalence Ratio (Φ)	0.7	1

Results and Discussion

For the optimization process it was used Matlab® R2015a Optimization Toolbox [57], which yields the following results for the Genetic Algorithm:

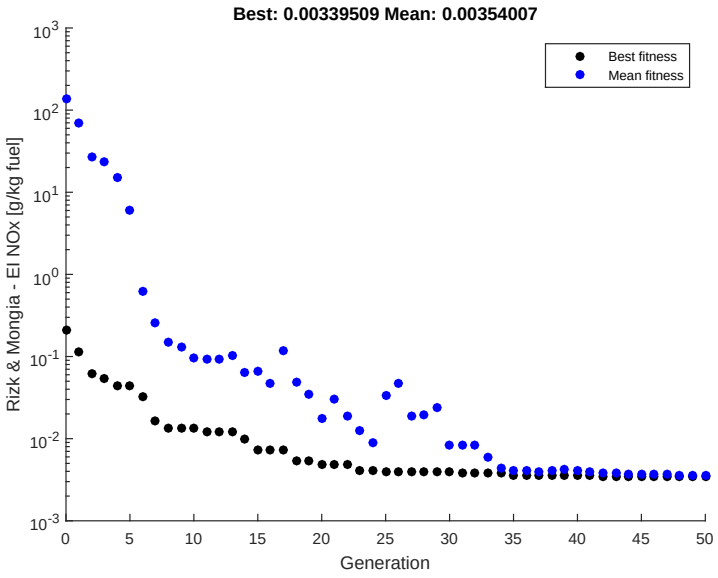

Figure 5.1: Single-Objective Optimization process.

As can be seen in figure 5.1 the algorithm has converged to an optimal fitness solution after about 50 generations. The optimal values of the parameters that were found by the algorithm are presented in the following table 5.2.

Table 5.2: Single-Objective Optimization results.

Parameters	Optimized values
Fan Pressure Ratio (FPR)	1.0032
Compressor Pressure Ratio (CPR)	10.0016
Residence time in ms (t_i)	0.1038
Equivalence Ratio (Φ)	0.7051
$EI_{NO_x total}$	0.0034

The results demonstrate that for an optimal solution on NO_x emissions only, the design parameters would have to be kept at minimum values. These results were expected since that the lower compression of the core air implicates a lower temperature at the inlet of the combustor and therefore a lower

temperature of combustion, the short residence time implicates that the combustion gases do not stay too much time at high temperatures and a low equivalence ratio yield lower flame temperatures, thus resulting in low NO_x emissions.

5.1.2 Multi-Objective Optimization

As mentioned before, the sole objective of minimizing the NO_x emissions is not enough for design purposes. Instead a Multi-objective approach is the norm, while trying to also minimize fuel consumption. This approach requires to define a second objective function so a compromise can be made in the selection of the optimal design parameters. Also, with the addition of a new objective function there is an increase in the number of parameters to consider since fuel consumption is also function of B and TIT that were omitted in the previous optimization.

$$EI_{NO_x total} = f(FPR, CPR, ti, \Phi) \tag{5.2a}$$

$$SFC = f(FPR, CPR, ti, \Phi, TIT, B) \tag{5.2b}$$

The constrains for the Multi-Objective optimization are also define in the following table 5.3.

Table 5.3: Design Parameters limits.

Parameters	Lower limit	Upper limit
Fan Pressure Ratio (FPR)	1	2
Compressor Pressure Ratio (CPR)	10	50
Residence time in ms (t_i)	0.1	10
Equivalence Ratio (Φ)	0.7	1
Turbine Inlet Temperature in K(TIT)	1500	2000
Bypass Ratio (B)	1	12

Results and Discussion

The following results for the NO_x emissions and Specific Fuel Consumption were obtained using Matlab's Optimization Toolbox originating a Pareto front where a decision upon the trade-offs between the two objective function can be made.

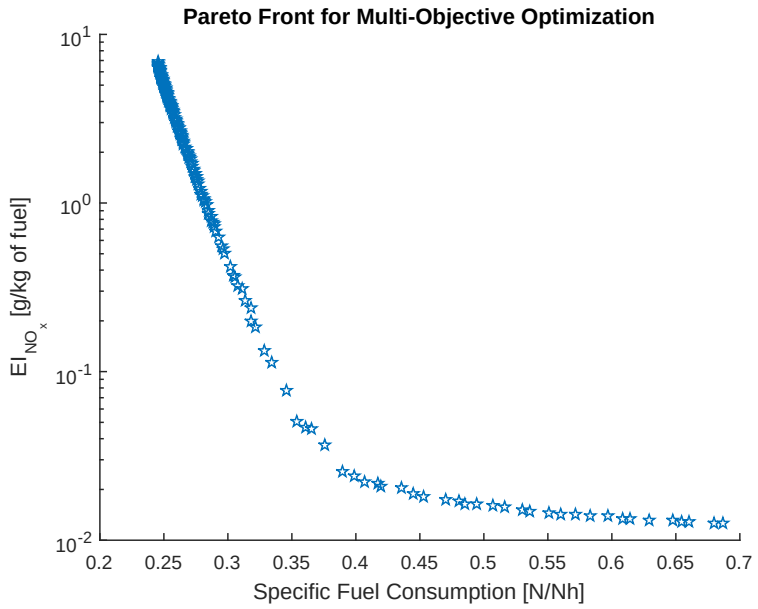

Figure 5.2: Multi-Objective Optimization Pareto front.

From the obtained optimized values, one can select sets of values that correspond to minimal fuel consumption, minimal NO_x emissions and a compromise between both. The choice of the compromised optimization is tackled by the analysis of the pareto front, where the optimal couple of SFC and EI_{NO_x} should be chosen from the set of values closer to the origin of the plot, where each objective can be simultaneously presented closer to their minimum without a significant variation of the other. These sets of values are presented in the following table.

Table 5.4: Multi-Objective Optimization results.

Parameters	**Minimum SFC**	**Minimum EI_{NO_x}**	**Optimal**
Fan Pressure Ratio (FPR)	1.3238	1.0838	1.3880
Compressor Pressure Ratio (CPR)	48.6066	10.1085	15.0505
Residence time in ms (t_i)	0.1126	0.1009	0.1074
Equivalence Ratio (Φ)	0.7056	0.7009	0.7021
Turbine Inlet Temperature in K(TIT)	1616.1	1622.2	1620.5
Bypass Ratio (B)	10.9235	10.7567	10.9183
Specific Fuel Consumption in N/Nh	0.2458	0.6869	0.3346
EI_{NO_x} in $g/kgfuel$	6.8414	0.0125	0.1124

The results can be analyzed by reviewing the values in table 5.4. A minimum SFC is obtained by high compression ratios yielding high temperatures in the combustor, thus increasing thermal and combustion efficiency, but increasing NO_x. For the minimum NO_x emissions, on the other hand, is achieved by low compression ratio, thus yielding low temperatures in the combustor. Optimal values for SFC and NO_x can be achieved by compromising on the optimized parameters. The overall compression ratio is kept in the middle of the values for minimum SFC and EI_{NO_x}, although FPR increases favoring the thrust generated by the bypass flow while alleviating the compression made by the compressor stage, thus resulting in better SFC and NO_x emissions. Residence time and Equivalence ratio are kept at a minimum so that low values of NO_x emissions can be achieved, denoting the

high sensitivity of NO_x formation to this parameters. The TIT is also kept at a minimum resulting in lower SFC. In concordance with the values for FPR, the values for the Bypass ratio are also kept at a maximum providing a higher percentage of air to go through the bypass flow, thus favoring the thrust generated from the fan and decreasing SFC.

5.2 Analysis of Optimized Engine with the proposed Combustion Model

The results obtained in the previous chapter, were derived from the a less computationally demanding Rizk $\&$ Mongia model. This provided a less time consuming optimization, although, it also provided a less extent analysis of the combustion process. For this matter, the proposed combustion model can now be used to provide the extra data which could not be extracted by the semi-empirical model.

Applying the optimized parameters from table 5.4 to the developed combustion model, yields the results that can be examined in the following table.

Table 5.5: Multi-Objective Optimization results applied to the developed model.

Parameters	**Minimum SFC**	**Minimum EI$_{NO_x}$**	**Optimal**
Fan Pressure Ratio (FPR)	1.3238	1.0838	1.3880
Compressor Pressure Ratio (CPR)	48.6066	10.1085	15.0505
Residence time in ms (t_i)	0.1126	0.1009	0.1074
Equivalence Ratio (Φ)	0.7056	0.7009	0.7021
Turbine Inlet Temperature in K(TIT)	1616.1	1622.2	1620.5
Bypass Ratio (B)	10.9235	10.7567	10.9183
Mole fraction in ppm			
CO_2	91967	94157	93810
H_2O	89654	89873	89862
H_{2e}	460.6	111.3	176.5
CO_e	2890.3	563.2	977.2
OH_e	4606.6	1668.5	2336.4
H_e	119.3	17.5	32.4
NO	2609.2	6.8	55.5
Specific Fuel Consumption in N/Nh	0.2458	0.6869	0.3346
EI$_{NO_x}$ in $g/kgfuel$	59.4007	0.1558	1.2645

Although it is beyond the scope of this thesis to analyze the formation of trace species other then NO_x, the equilibrium concentrations of the several radicals and other trace species are obtain as result of the calculations made in the model.

For instance, the equilibrium concentration of the carbon monoxide is given by the made calculations, while computing the combustion process. For the incomplete reaction, CO is formed by the dissociation of CO_2 in the high temperatures at the flame. By resorting to the literature [51], it is verified that for the range of residence times and equivalence ratio used throughout the analysis, the equilibrium condition is achieved for CO.

Although this analysis do not provide the complete review of the CO formation process, it is important to retrieve the maximum information from the expressed results, including the contributions of

the equilibrium CO in emissions. In practice, CO emissions arises from incomplete combustion and are found to be much higher than predicted from the equilibrium analysis. Nevertheless, analyzing the results in table 5.4 provide a good qualitative insight of the influence which a low NO_x focused design analysis have on CO equilibrium concentration. Thus, it can be noted that low specific fuel consumption oriented design optimization yield higher CO equilibrium concentrations than the low NO_x approach. This is justified by the high temperatures, achieved by the high compression imposed by the SFC optimized parameters, which promote the incomplete combustion effects. Analogously, and as noted in the results and discussion of chapter 5.1, the NO concentration also increases from the low NO_x optimized parameters to the low SFC optimized parameters. Of major importance, is to denoted that the formation of the NO_x increases by a factor of 400 when exchanging from low NO_x setup to a low SFC setup, while CO equilibrium concentrations just increase by a factor of 5, thus proving the high sensibility of NO_x formation to the parameters variation.

6

Conclusions and Future Work

Contents

6.1 Conclusions

In the present thesis the objectives proposed in section 1.3 were accomplished with success. A complete model of a two-spool turbofan was formulated and validated with good agreement with both commercial software results, with mean relative differences of 4% to specific fuel consumption and 10% to specific thrust, and real data retrieved from ICAO engine data bank, with mean relative differences of 14% when comparing with the retrieved values specific fuel consumption. Furthermore a theoretical combustion model was formulated for the primary zone and NO_x formation mechanism, and validated throughout the formulation process with very good results, presenting relative differences of less then 1% when calculating the adiabatic flame temperature and less then 3% when calculating the concentration of the products of combustion. The proposed turbofan model was then paired with both the proposed combustion model and semi-empirical model available from the literature, namely Rizk $\&$ Mongia model providing the computational simplicity needed in order to proceed with the optimization process. Both turbo-emissions models yield very good results when compared with data retrieved from ICAO emissions data bank. Because it shown more computationally demanding the optimization process was carried out by the conjoint model of the turbofan and the Rizk $\&$ Mongia model instead of using the proposed combustion model. Nevertheless, the optimization process led to realistic results, yielding three different sets of optimized performance parameters, the first two sets representing results for the two different objectives of low specific fuel consumption and low NO_x emissions, and a third set representing an optimal compromise between the former two sets. The set of optimal parameters proves to be of great advantage as NO_x emissions are greatly reduced, around 97% when comparing with the least favorable approach of the minimum specific fuel consumption objective, and a reduction of 50% in minimum specific fuel consumption when comparing with the least favorable approach of minimum NO_x emissions. The more computationally demanding combustion model was then used with the achieved optimized performance parameters, in order to compute the NO_x emissions. With a stronger theoretical background, the model provided additional information about the formation of trace species other than NO_x.

6.2 Future Work

Within the 0D framework, future work can be assessed by the development of additional models regarding other types of aircraft engines. A new combustion model could be developed accommodating the formation of other pollutants within the same 0D framework, thus providing a more complete analysis without compromising the computational effort. Finally, in order to provide a complete optimization of the engine, other than low NO_x emissions and low fuel consumption objectives have to be traced. The more complex optimization process would have to account with the reduction of other relevant trace species as well as operational and off design analysis.

Bibliography

[1] I. Secretariat, "Aircraft technology improvements," *ICAO Environmental Report*, 2013.

[2] E. A. S. Agency, "European aviation environmental report," EASA, Tech. Rep., 2016.

[3] W. Dodds, "Engine and aircraft technologies to reduce emissions," *ICCAIA Noise and Emissions Committee, San Diego*, vol. 1, 2002.

[4] S. Samuelsen, "Rich burn, quick-mix, lean burn (RQL) combustor," *The Gas Turbine Handbook, US Department of Energy, Office of Fossil Energy, National Energy Technology Laboratory, DOE/NETL2006-1230*, pp. 227–233, 2006.

[5] C. T. Chang, "Low-emissions combustors development and testing," 2012.

[6] D. S. Lee, D. W. Fahey, P. M. Forster, P. J. Newton, R. C. Wit, L. L. Lim, B. Owen, and R. Sausen, "Aviation and global climate change in the 21st century," *Atmospheric Environment*, vol. 43, no. 22, pp. 3520–3537, 2009.

[7] I. Isaksen, C. Jackman, S. Baughcum, F. Dentener, W. Grose, P. Kasibhatla, D. Kinnison, M. Ko, J. McConnell, G. Pitari *et al.*, "Modeling the chemical composition of the future atmosphere," 1999.

[8] R. Derwent and R. Friedl, "Impacts of aircraft emissions on atmospheric ozone," *IPCC Special Report on Aviation and the Global Atmosphere*, pp. 29–64, 1999.

[9] P. Minnis, U. Schumann, D. R. Doelling, K. M. Gierens, and D. W. Fahey, "Global distribution of contrail radiative forcing," *Geophysical Research Letters*, vol. 26, no. 13, pp. 1853–1856, 1999.

[10] G. Pitari, E. Mancini, V. Rizi, and D. Shindell, "Impact of future climate and emission changes on stratospheric aerosols and ozone," *Journal of the Atmospheric Sciences*, vol. 59, no. 3, pp. 414–440, 2002.

[11] J. Riess, *NO_x: how nitrogen oxides affect the way we live and breathe*. US Environmental Protection Agency, Office of Air Quality Planning and Standards, 1998.

[12] S. W. Nixon, "Coastal marine eutrophication: a definition, social causes, and future concerns," *Ophelia*, vol. 41, no. 1, pp. 199–219, 1995.

[13] S. Solomon, D. Qin, M. Manning, Z. Chen, M. Marquis, K. Averyt, M. Tignor, and H. Miller, "IPCC fourth assessment report (ar4)," *Retrieved*, vol. 4, no. 13, p. 2011, 2007.

[14] J. Faber, D. Greenwood, D. Lee, M. Mann, P. M. De Leon, D. Nelissen, B. Owen, M. Ralph, J. Tilston, A. van Velzen *et al.*, "Lower NO_x at higher altitudes policies to reduce the climate impact of aviation NO_x emission," *CE Delft Solutions for environment, economy and technology*, 2008.

[15] T. C. Lieuwen and V. Yang, *Gas turbine emissions*. Cambridge University Press, 2013, vol. 38.

[16] P. . Whitney and G. Electric, "Critical propulsion components volume 2: Combustor," *NASA CR-2005-213584*, 2005.

[17] V. Jermakian, V. McDonell, G. Samuelsen, C. E. Commission *et al.*, *Experimental Study of the Effects of Elevated Pressure and Temperature on Jet Mixing and Emissions in an RQL Combustor for Stable, Efficient and Low Emissions Gas Turbine Applications: Final Project Report*. California Energy Commission, 2012.

[18] G. Howe, Z. Li, T. Shih, and H. Nguyen, "Simulation of mixing in the quick quench region of a rich burn-quick quench mix-lean burn combustor," *AIAA Paper*, no. 91-0410, 1991.

[19] M. C. Cline, G. J. Micklow, S. Yang, and H. Nguyen, "Numerical analysis of the flowfields in a staged gas turbine combustor," *Journal of Propulsion and Power*, vol. 11, no. 5, pp. 894–898, 1995.

[20] M. Talpallikar, C. Smith, M. Lai, and J. Holdeman, "CFD analysis of jet mixing in low NO_x flame-tube combustors," *Journal of Engineering for Gas Turbines and Power*, vol. 114, no. 2, pp. 416–424, 1992.

[21] M. Blomeyer, B. Krautkremer, D. Hennecke, and T. Doerr, "Mixing zone optimization of a rich-burn/quick-mix/lean-burn combustor," *Journal of Propulsion and Power*, vol. 15, no. 2, pp. 288–295, 1999.

[22] D. Mavris *et al.*, "Enhanced emission prediction modeling and analysis for conceptual design," *Final Report for NASA grant NNX07AO08A*, vol. 17, 2010.

[23] H. C. Mongia, "Taps: A fourth generation propulsion combustor technology for low emissions," *AIAA paper*, vol. 2657, p. 2003, 2003.

[24] L. Matuszewski, F. Dupoirieux, C. Guin, and F. Grisch, "Numerical calculation of the no formation in a multi-point combustion chamber and results of the associated validation experiments," in *9th Onera-DLR Aerospace Symposium*, 2008.

[25] G. Sturgess and K.-Y. Hsu, "Combustion characteristics of a trapped vortex combustor," in *RTO Meeting proceedings*, 1999.

[26] C. Bruno and M. Losurdo, "The trapped vortex combustor: an advanced combustion technology for aerospace and gas turbine applications," in *Advanced combustion and aerothermal technologies*. Springer, 2007, pp. 365–384.

[27] D. Mishra, *Fundamentals of combustion*. PHI Learning Pvt. Ltd., 2007.

[28] P. C. Mancilla, P. Chakka, and S. Acharya, "Performance of a trapped vortex spray combustor," in *ASME Turbo Expo 2001: Power for Land, Sea, and Air*. American Society of Mechanical Engineers, 2001, pp. V002T02A025–V002T02A025.

[29] F. Xing, S. Zhang, P. Wang, and W. Fan, "Experimental investigation of a single trapped-vortex combustor with a slight temperature raise," *Aerospace Science and Technology*, vol. 14, no. 7, pp. 520–525, 2010.

[30] F. Xing, P. Wang, S. Zhang, J. Zou, Y. Zheng, R. Zhang, and W. Fan, "Experiment and simulation study on lean blow-out of trapped vortex combustor with various aspect ratios," *Aerospace Science and Technology*, vol. 18, no. 1, pp. 48–55, 2012.

[31] J. Bucher, R. G. Edmonds, R. C. Steele, D. W. Kendrick, B. C. Chenevert, and P. C. Malte, "The development of a lean-premixed trapped vortex combustor," in *ASME Turbo Expo 2003, collocated with the 2003 International Joint Power Generation Conference*. American Society of Mechanical Engineers, 2003, pp. 207–213.

[32] A. Lefebvre, "Fuel effects on gas turbine combustion - ignition, stability, and combustion efficiency," *Journal of Engineering for Gas Turbines and Power*, vol. 107, no. 1, pp. 24–37, 1985.

[33] A. H. Lefebvre, D. R. Ballal *et al.*, *Gas turbine combustion*. CRC Press, 2010.

[34] N. Rizk and H. Mongia, *Emissions predictions of different gas turbine combustors*, ser. Aerospace Sciences Meetings. American Institute of Aeronautics and Astronautics, Jan 1994.

[35] K. Rink and A. Lefebvre, "The influences of fuel composition and spray characteristics on nitric oxide formation," *Combustion Science and Technology*, vol. 68, no. 1-3, pp. 1–14, 1989.

[36] K. G. Kyprianidis, D. Nalianda, and E. Dahlquist, "A NO_x emissions correlation for modern RQL combustors," *Energy Procedia*, vol. 75, pp. 2323–2330, 2015.

[37] K. G. Kyprianidis, "Multi-disciplinary conceptual design of future jet engine systems,"*Cranfield University*, 2010.

[38] A. Mellor, "Semi-empirical correlations for gas turbine emissions, ignition, and flame stabilization," *Progress in Energy and Combustion Science*, vol. 6, no. 4, pp. 347–358, 1980.

[39] G. D. Lewis, "A new understanding of NO_x formation," in *Tenth International Symposium on Air-Breathing Engines*, no. 625-9. Nottingham, UK: AIAA, Washington, DC, 1991.

[40] J. Odgers and D. Kretschmer, "The prediction of thermal NO_x in gas turbines," in *ASME 1985 Beijing International Gas Turbine Symposium and Exposition*. American Society of Mechanical Engineers, 1985, pp. V002T04A022–V002T04A022.

[41] T. Becker and M. Perkavec, “The capability of different semianalytical equations for estimation of NO_x emissions of gas turbines,” in *ASME 1994 International Gas Turbine and Aeroengine Congress and Exposition*. American Society of Mechanical Engineers, 1994, pp. V003T06A020–V003T06A020.

[42] D. G. Nicol, P. C. Malte, and R. C. Steele, “Simplified models for NO_x production rates in lean-premixed combustion,” in *ASME 1994 International Gas Turbine and Aeroengine Congress and Exposition*. American Society of Mechanical Engineers, 1994, pp. V003T06A037–V003T06A037.

[43] P. Norman, D. Lister, M. Lecht, P. Madden, K. Park, O. Penanhoat, C. Plaisance, and K. Renger, “Development of the technical basis for a new emissions parameter covering the whole aircraft operation: Nepair,” *European Commission, Rept. G4RD-CT-2000-00182, Brussels*, 2003.

[44] N. R. C. U. C. to Study the Impact of Information Technology on the Performance of Service Activities, N. R. C. U. C. Science, T. Board, N. R. C. U. C. on Physical Sciences, Mathematics, and Applications, *Information technology in the service society: A twenty-first century lever*. National Academies Press, 1994.

[45] M. Cavcar, “The international standard atmosphere (ISA),” *Anadolu University, Turkey*, vol. 30, 2000.

[46] J. Mattingly, *Elements of Gas Turbine Propulsion*, ser. McGraw-Hill series in aeronautical and aerospace engineering. McGraw-Hill, 1996.

[47] J. Kurzke, “GasTurb 12 user’s manual,” *GasTurb GmbH, Dachau, Germany*, 2013.

[48] ICAO, “Aircraft engine emissions databank,” Doc 9646-AN/943, Tech. Rep., 2015.

[49] I. Glassman, R. Yetter, and N. Glumac, *Combustion*. Elsevier Science, 2014.

[50] K. Denbigh, *The Principles of Chemical Equilibrium: With Applications in Chemistry and Chemical Engineering*. Cambridge University Press, 1981.

[51] R. Flagan and J. Seinfeld, *Fundamentals of Air Pollution Engineering*, ser. Dover Civil and Mechanical Engineering. Dover Publications, 2013.

[52] R. K. Hanson and S. Salimian, “Survey of rate constants in the N/H/O system,” in *Combustion chemistry*. Springer, 1984, pp. 361–421.

[53] G. A. Lavoie, J. B. Heywood, and J. C. Keck, “Experimental and theoretical study of nitric oxide formation in internal combustion engines,” *Combustion Science and Technology*, vol. 1, no. 4, pp. 313–326, 1970.

[54] J. M. Seitzman, “Chemical kinetics: Analyzing reaction mechanisms.,”*Georgia Tech Georgia Institute of Technology*, 2004.

[55] D. Lentini, “Modelling the nitrous oxide pathway contribution to NO, in nonpremixed turbulent flames,” in *WIP presentation at the 28th Symp.(Int.) on Combust., Edinburgh*, 2000.

[56] D. Lentini, “Prediction of NO_x emissions in gas turbine combustors inclusive of the N_2O contribution,” *Proceedings of the Institution of Mechanical Engineers, Part A: Journal of Power and Energy*, vol. 217, no. 1, pp. 83–90, 2003.

[57] A. Chipperfield and P. Fleming, “The MATLAB genetic algorithm toolbox,” in *Applied control techniques using MATLAB, IEE Colloquium on*. IET, 1995, pp. 10–1.

Appendix

A.1 Characteristic time comparison

$$1) \quad N_2 + O \rightleftharpoons NO + N \tag{A.1}$$

$$2) \quad N + O_2 \rightleftharpoons NO + O \tag{A.2}$$

Table A.1: Comparison of characteristic times CH_4 at 1 atm.

	1000 K	**1500** k	**2000** k
t_{1f}	$3\times10^{-3}s$	$100s$	$0.2s$
t_{2f}	$2\mu s$	$0.5\mu s$	$0.2\mu s$

As can be denoted the chain reaction is limited by the formation of the radical N by the first reaction, which is orders of magnitude slower.

A.2 Combustion Model Validation using CH_4 as a fuel

In this Annex, an incomplete combustion with dissociation products derived from combustion equilibrium is analyzed. The fuel used is the same heavy fuel oil, CH_4, under the initial conditions, $P_0 = 1$ atm and $T_0 = 298$ K, and $\Phi = 1$.

Table A.2: Comparison of results for a incomplete combustion of CH_4 at 1 atm and 298 K.

Evaluated Entities	**Reference**	**Model**	**Relative Error**
Mole fractions			
N_2	0.7103	0.7115	0.17%
CO_2	0.0854	0.0854	-0.02%
O_2	6.34×10^{-3}	6.20×10^{-3}	-2.16%
H_2O	0.1853	0.1846	-0.36%
CO	9.04×10^{-3}	8.70×10^{-3}	-3.76%
H_2	3.63×10^{-3}	3.70×10^{-3}	1.82%
Adiabatic Flame Temperature in K	2252.35	2265.8	0.6%

The model shows to validate well when faced with incomplete combustion, providing accurate estimates with relative errors inferior to 3%.